

Contract No:

This document was prepared in conjunction with work accomplished under Contract No. DE-AC09-08SR22470 with the U.S. Department of Energy (DOE) Office of Environmental Management (EM).

Disclaimer:

This work was prepared under an agreement with and funded by the U.S. Government. Neither the U. S. Government or its employees, nor any of its contractors, subcontractors or their employees, makes any express or implied:

- 1) warranty or assumes any legal liability for the accuracy, completeness, or for the use or results of such use of any information, product, or process disclosed; or
- 2) representation that such use or results of such use would not infringe privately owned rights; or
- 3) endorsement or recommendation of any specifically identified commercial product, process, or service.

Any views and opinions of authors expressed in this work do not necessarily state or reflect those of the United States Government, or its contractors, or subcontractors.

We put science to work.™



**Savannah River
National Laboratory®**

OPERATED BY SAVANNAH RIVER NUCLEAR SOLUTIONS

A U.S. DEPARTMENT OF ENERGY NATIONAL LABORATORY • SAVANNAH RIVER SITE • AIKEN, SC

Fabricating and Testing Additively Manufactured Components for Tritium Service Consideration

P. Korinko, J. Bobbitt III, S. Scott, & K. Shanahan

Sept. 2020

SRNL-STI-2020-00358, Revision 1

SRNL.DOE.GOV

DISCLAIMER

This work was prepared under an agreement with and funded by the U.S. Government. Neither the U.S. Government or its employees, nor any of its contractors, subcontractors or their employees, makes any express or implied:

1. warranty or assumes any legal liability for the accuracy, completeness, or for the use or results of such use of any information, product, or process disclosed; or
2. representation that such use or results of such use would not infringe privately owned rights; or
3. endorsement or recommendation of any specifically identified commercial product, process, or service.

Any views and opinions of authors expressed in this work do not necessarily state or reflect those of the United States Government, or its contractors, or subcontractors.

Printed in the United States of America

**Prepared for
U.S. Department of Energy**

Keywords: *Hydrogen, Tritium, Tooling,
Additive Manufacturing*

Retention: *Permanent*

Fabricating and Testing Additively Manufactured Components for Tritium Service Consideration

P. Korinko, J. Bobbitt, S. Scott, & K.
Shanahan

Sept. 2020

Prepared for the U.S. Department of Energy under
contract number DE-AC09-08SR22470.



OPERATED BY SAVANNAH RIVER NUCLEAR SOLUTIONS

REVIEWS AND APPROVALS

Author: P. Korinko	Signature:	Organization: SRNL-L8200
Author: J. Bobbitt	Signature:	Organization: SRNL-L4500
Author: S. Scott	Signature:	Organization: SRNL-L3330
Author: K. Shanahan	Signature:	Organization: SRNL-L2110
Technical Reviewer: A. McWilliams	Signature:	Organization: SRNL-L8200
Manager: Laura Tovo	Signature:	Organization: SRNL-L8200
Customer: P. Foster	Signature:	Organization: SRNS-T3940

PREFACE OR ACKNOWLEDGEMENTS

This project was conducted as part of the Savannah River Tritium Enterprise (SRTE) Plant Manager Directed Research and Development (PDRD) projects. This project has had support from a number of people including Patrick Kuzbary, Tony Curtis, Tim Krentz, Travis Hubbard, Max Housley, Jeff Steedley, and the staff at the 749-A machine shop.

EXECUTIVE SUMMARY

This SRTE PDRD sponsored project produced test articles, tooling, and training articles for evaluation. In addition, the hydrogen compatibility of the alloys that can be readily produced by the Arcam A2X was tested. During the evaluation it was determined that the mechanical properties were more sensitive to build plate location than hydrogen exposure. Hydrogen pressure – volume- temperature experiments showed that the as-fabricated samples did not absorb hydrogen readily, but activated samples did.

TABLE OF CONTENTS

LIST OF TABLES	viii
LIST OF FIGURES	viii
LIST OF ABBREVIATIONS.....	x
1.0 Introduction.....	1
2.0 Approach.....	3
2.1 Test article printing	3
2.2 Metallography	4
2.3 Hydrogen charging	4
2.4 Mechanical Properties Testing.....	7
2.5 Fractography.....	8
2.6 PVT testing.....	8
3.0 Results.....	9
3.1 Printed Objects	9
3.2 Metallography	11
3.3 Hydrogen Charging	12
3.4 Mechanical Properties	14
3.4.1 SEM fractography.....	18
3.5 PVT Testing	19
3.5.1 Ti64_1.....	19
3.5.2 Ti64_2.....	21
3.5.3 Ti64_3.....	22
3.5.4 Ti64_4.....	22
3.5.5 Ti64_5.....	24
4.0 Conclusions.....	25
5.0 Recommendations, Path Forward or Future Work	25
6.0 References.....	25
Appendix A . Detailed Results Hydrogen Charging and Tensile Testing	A-1

LIST OF TABLES

Table 2-1 Hydrogen Charging Vessels Initial Loading	6
Table 2-2 Example Hydrogen Exposure Vessel Contents and Conditions.....	6
Table 2-3. Sample weights before and after processing and sample condition tested	9
Table 3-1 Hydride on-set temperature for hydriding	24
Table 6-1 Hydrogen Exposure Vessel Contents and Conditions	A-1

LIST OF FIGURES

Figure 1-1. The PBF-EB system is comprised of an electron beam gun, column with focusing and deflecting electromagnetic lenses, a powder distribution system, and the powder bed.....	1
Figure 1-2 The Arcam process is comprised of a number of steps as shown above.....	2
Figure 1-3 Photos showing the parts removal and cleaning evolution for some lattices printed for a NA-115 project.	3
Figure 1-4 Arcam A2X installed in SRNL in the Additive Manufacturing Development Laboratory.....	3
Figure 2-1 Build plate design for samples used for hydrogen testing and blocks used provided for microstructure examination at Colorado School of Mines.	4
Figure 2-2 Photos of an assembled conflat flange vessel used for hydrogen charging	5
Figure 2-3 Photos of example speckle patterns applied to tensile specimens in the as-printed condition (left) and as machined (right).	7
Figure 2-4 Example strain map of a tensile specimen generated using digital image correlation.	8
Figure 3-1 Simulated valves, tensile samples on the build plate and separated from it in the as-printed condition, a Dremel too stem cut-off holder, and a light weight fuel cell holder article.	10
Figure 3-2 This image shows a print job that was interrupted / failed due to swelling, the job was continued from the stop point rather than restarting the job.....	11
Figure 3-3 Longitudinal section of showing the extended beta grains from low to high magnification ...	12
Figure 3-4 Transverse cross-section of as-fabricated Ti64.....	12
Figure 3-5 Transverse cross-sections showing the lack of alpha phase formation for an Ar exposed sample.	13
Figure 3-6 Longitudinal cross-section of an Ar exposed Ti64 sample.	13
Figure 3-7 Transverse sample metallography after hydrogen exposure at 200C for 6 weeks showing the lack the hydride formation.....	14
Figure 3-8 Longitudinal cross-section of a sample exposed to hydrogen for six weeks at 200°C.	14

Figure 3-9 Tensile property comparison of samples exposed to 3% hydrogen in argon at 200 °C for 7 weeks and argon at 100 °C for 11 weeks.....	15
Figure 3-10 Tensile property comparison of samples exposed to 3% and 1% hydrogen environments at 200 °C for 7 weeks.	15
Figure 3-11 Tensile property comparison of samples exposed to 1% hydrogen in argon at 100 °C and 200 °C for 7 weeks.	16
Figure 3-12 Tensile property comparison of samples printed at the “middle” build position under varying exposure conditions.	17
Figure 3-13 Low-magnification fractography of a tensile specimen in the as-printed condition	17
Figure 3-14 Low-magnification fractography of a tensile specimen in the machine-printed condition....	18
Figure 3-15 Sample D1, as printed from the high position, after exposure at 3% H ₂ at 200 C for 7 weeks.	18
Figure 3-16 Sample D2, machined from the high position, after exposure to 3% H ₂ at 200 °C for 7 weeks.	19
Figure 3-17 Sample D5, as-printed from low position, after exposure to 3% H ₂ at 200 °C for 7 weeks...	19
Figure 3-18 Sample D6, machined sample from low position, after exposure at 3% H ₂ at 200 °C for 7 weeks.	19
Figure 3-19 Raw data for hydriding sample Ti64_1	20
Figure 3-20 Pressure vs. sample temperature during heating (Ti64_1)	21
Figure 3-21 PVT testing form sample Ti64_2	22
Figure 3-22 Ti64_3 Hydriding occurred after heating to over 400°C.	23
Figure 3-23 Pressure and temperature plot for the sample Ti64_4 showing hydriding at lower temperatures than with machined surfaces.....	23
Figure 3-24 Preheating samples to activate the surface results in hydriding at significantly lower temperatures.....	24
Figure 6-1 Tensile properties of vessel 1 samples, 3% hydrogen in argon, 200 °C for 7 weeks.....	A-2
Figure 6-2 Tensile properties of vessel 2 samples, 1% hydrogen in argon, 200 °C for 7 weeks.....	A-2
Figure 6-3 Tensile properties of vessel 3 samples, 1% hydrogen in argon, 200 °C for 11 weeks.....	A-3
Figure 6-4 Tensile properties of vessel 4 samples, 1% hydrogen in argon, 100 °C for 7 weeks.....	A-3
Figure 6-5 Tensile properties of vessel 5 samples, 1% hydrogen in argon, 100 °C for 11 weeks.....	A-4
Figure 6-6 Tensile properties of vessel 6 samples, argon, 100 °C for 11weeks.	A-4
Figure 6-7. Tensile properties of vessel 7 samples, argon, 200 °C for 11weeks.	A-5

LIST OF ABBREVIATIONS

AM	Additive Manufacturing
BP	Build Plate
CoCr	Cobalt 20% Chromium
DED	Direct Energy Deposition
DIC	Digital Image Correlation
EB	Electron Beam
PBF	Powder Bed Fusion
PDRD	Plant Manager Directed Research and Development
PRS	Powder Recovery System
PVT	Pressure Volume Temperature
SRNL	Savannah River National Laboratory
SRTE	Savannah River Tritium Enterprise
Ti64	Titanium 6% aluminum 4% vanadium

1.0 Introduction

Additive manufacturing is defined as a digital fabrication process where an engineering model, such as a computer aided design, is electronically processed by machine processing software, this output is then used to develop a toolpath which is downloaded to a 3D printer. The defined toolpath, beam path, heat source is then used by the printer to produce products that are at or near the final shape, i.e., net shape functional articles.

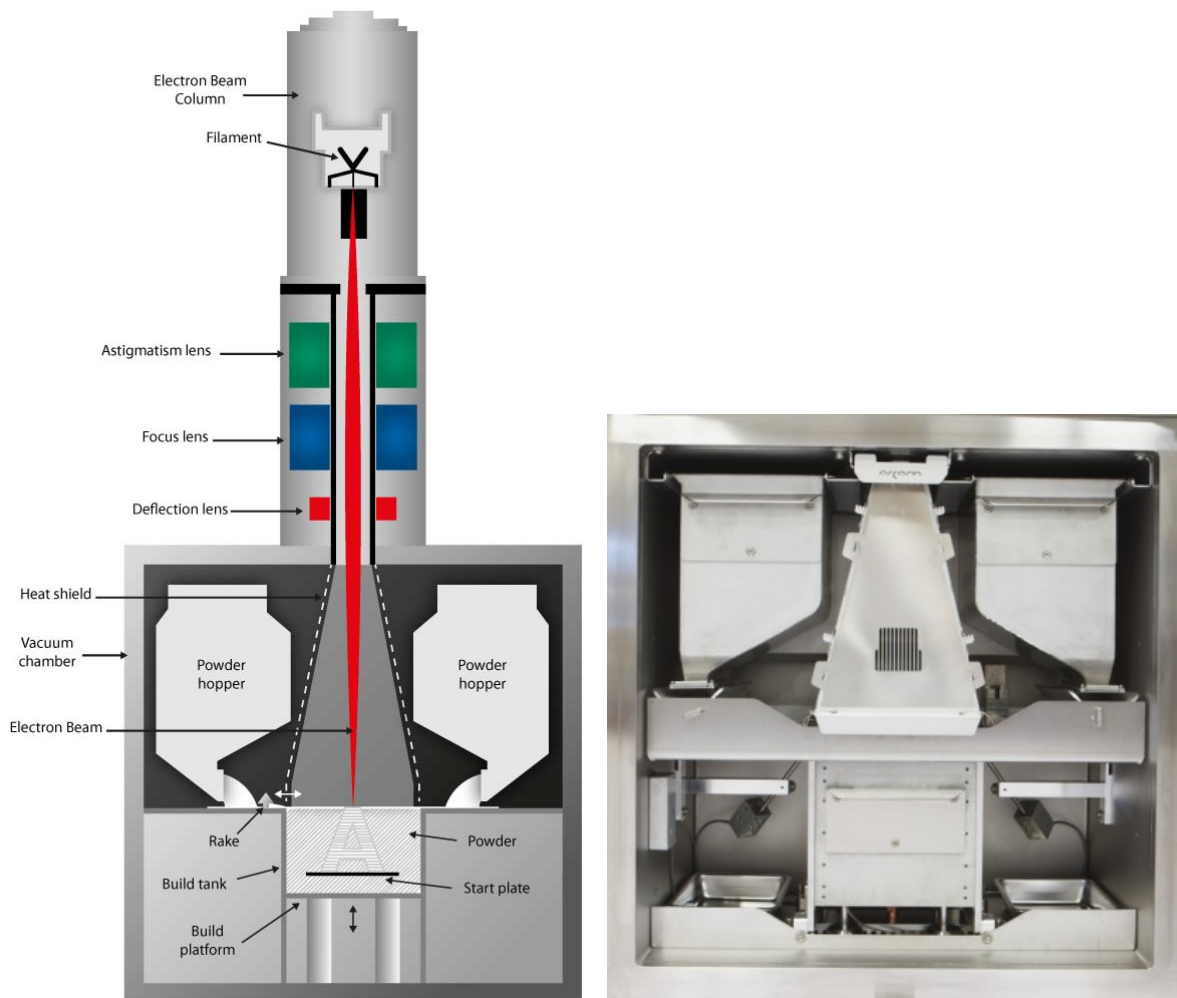
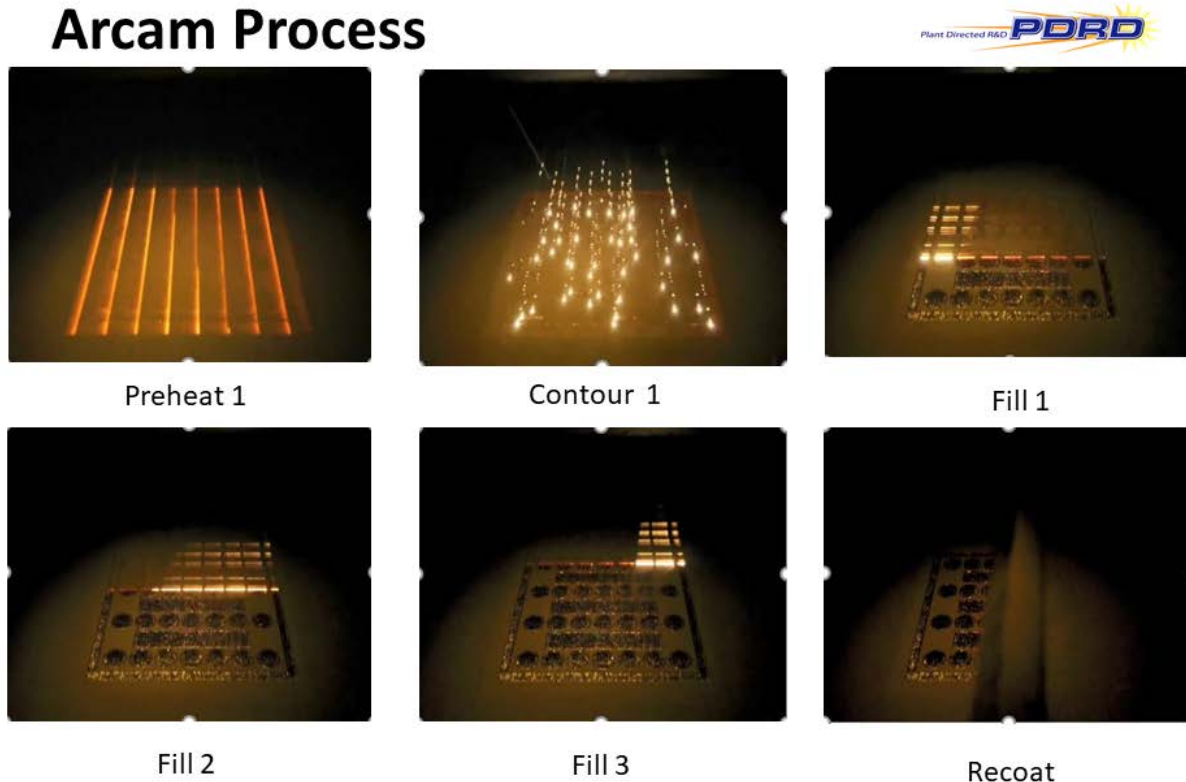


Figure 1-1. The PBF-EB system is comprised of an electron beam gun, column with focusing and deflecting electromagnetic lenses, a powder distribution system, and the powder bed.

AM is a maturing technology that has been described in a number of review articles (1-3) that describe the major processes. There are two primary processes used to produce metal AM components, directed energy deposition (DED) (either powder (P-DED) or wire fed (W-DED)) and powder bed fusion processes (PBF). PBF processes can typically use either laser (L-PBF) or electron beam (EB-PBF) heat sources.

Each process has positive and negative attributes, as do the machines from the various vendors. In this work, an electron beam powder bed fusion (EB-PBF) 3D printer manufactured by Arcam, a GE Additive Company, was used to produce tooling and test articles (shown schematically in Figure 1-1). It is comprised of an electron gun that operates in high vacuum in the 10^{-6} Torr range, a series of focusing electromagnetic lenses, a deflection lens, and a processing chamber. The processing vacuum chamber operates with a low flow of helium at a chamber pressure of about 5×10^{-4} Torr to reduce metal vaporization and contains powder hoppers, powder spreading system and rake, a vertically moveable build platform, and a build tank to contain the powder. The actual build chamber is also shown in Figure 1-1. The Arcam PBF-EB printing process is achieved by downloading build files to the control printer, loading the powder, completing the pre-job calibrations and verifications, placing a clean build plate on the build platform, preheating the plate and chamber to the desired temperature, raking powder across the plate, preheating the layer of powder, sintering the loose powder mass, melting the powder in the desired locations, and then repeating these last steps until the parts are built. Each layer is 50 μm thick, so a build can be several hundred to thousands of layers, Figure 1-2. The powder sintering step is required to ensure an electron path between the parts and earth, needed to ensure the particles do not scatter and cause deposits in the chamber. Once cooled, the sintered mass of powder is removed, and the sintered powder is blasted off in the powder recovery system (PRS). The PRS uses the same powder as the build chamber to blast off the sintered mass in order to eliminate cross contamination, it also allows for the powder to be reused. A print job removed from the printer in various states of processing is shown in Figure 1-3.

Arcam Process



Total process takes between 30 and 60 seconds per layer

Figure 1-2 The Arcam process is comprised of a number of steps as shown above

SRNL purchased and installed the Arcam A2X in 2017 (see Figure 1-4), for prototype tooling using standard parameters and also to be used as an open platform for fully trained SRNL scientists and engineers to develop new materials, new processing parameters, and new tool paths. Developers can optimize over 600 machine parameters to perform this activity.

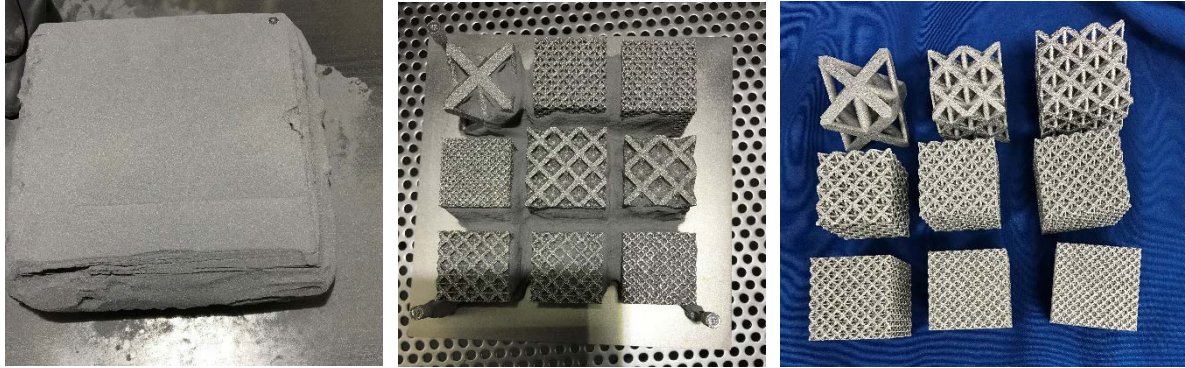


Figure 1-3 Photos showing the parts removal and cleaning evolution for some lattices printed for a NA-115 project.



Figure 1-4 Arcam A2X installed in SRNL in the Additive Manufacturing Development Laboratory.

A number of print runs were conducted to evaluate the form and fit of test parts to determine the suitability of the Arcam A2X for production of test articles and tooling for use in the SRTE facility. The mechanical properties of Ti64 test samples in the as-printed condition and after hydrogen exposure were characterized, the hydrogenation behavior was characterized using PVT testing.

2.0 Approach

2.1 Test article printing

Test articles and components were fabricated using the standard Arcam A2X parameters. These include: the software-generated beam paths, a layer thickness of 50 μm , a preheat temperature of 650°C, a beam

scan speed up to 8000 m/s that allows multiple melt pools, and using Ti - 6Al - 4V with a particle size range of 45 to 105 μm . A typical build plate for test articles is shown in Figure 2-1.

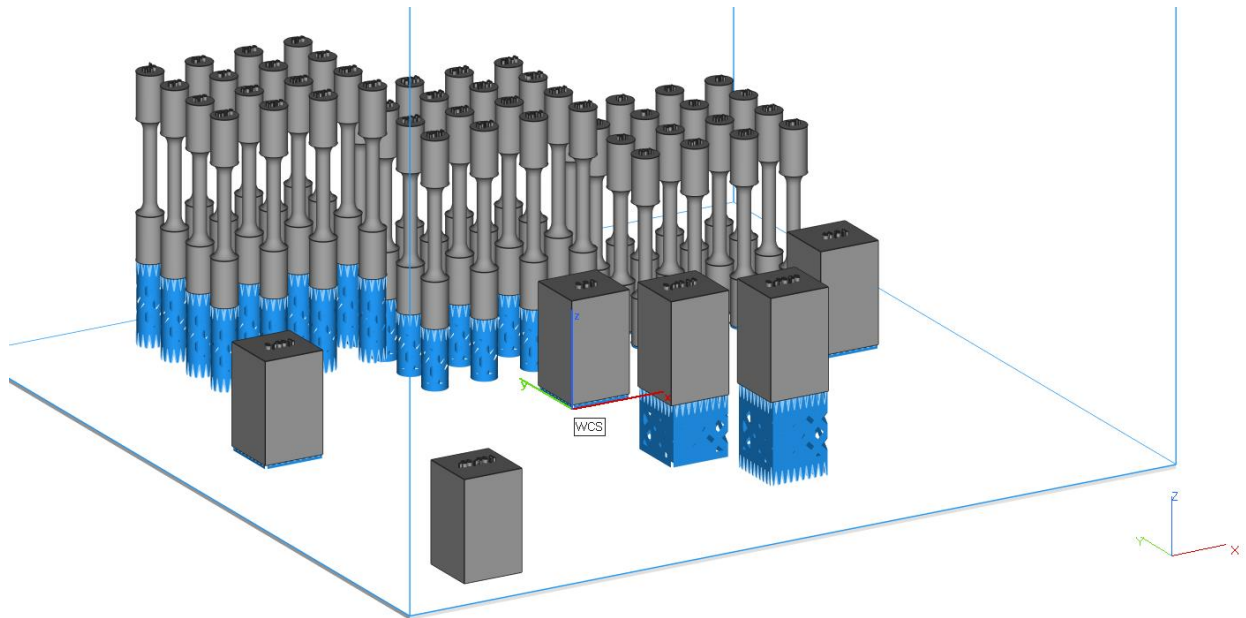


Figure 2-1 Build plate design for samples used for hydrogen testing and blocks used provided for microstructure examination at Colorado School of Mines.

2.2 Metallography

Metallographic samples were selectively prepared by cutting sections from tensile samples at several elevations on the samples in both the transverse and longitudinal orientation. Samples were mounted in epoxy, metallographically prepared using standard papers and diamond paste, chemically etched using Kroll's reagent, and photographed on a Keyence VHX 5000 microscope. The samples were examined and digitally imaged at low to high magnifications.

2.3 Hydrogen charging

Hydrogen charging of the tensile samples was accomplished by loading samples into conflat flange vessels, which were subsequently evacuated and backfilled with hydrogen and argon at varying pressures to meet the desired hydrogen atmospheres. The vessels used in this experiment were assembled from components which had been previously evaluated (calculation number M-CLC-H-03496) for pressure and temperature limits of 100 psig at 550 °F. Each vessel consisted of a 2.75" OD conflat flange spool, terminated by a 2.75" OD blank conflat flange and a CF to VCR adapter attached to a 1/4" VCR valve. The end caps were fastened using 1/4" hex head bolt and nut sets. All components used within the vessels were 304L SS, excluding the copper gaskets used in the knife-edge seal on the conflat flanges. An example assembled vessel is shown below in Figure 2-2.



Figure 2-2 Photos of an assembled conflat flange vessel used for hydrogen charging

The ideal gas law (Equation 1) was used to account for the change in pressure with temperature between the initial loading at room temperature 25 °C and a maximum temperature of 250 °C to account for potential overshoot during thermal transients versus the target maximum of 200 °C. To ensure that the maximum pressure of 95 psig at 250 °C was not exceeded, a maximum pressure of 85 psig was calculated for the maximum temperature of 200 °C. Accounting for the vessel volume of 200 ml, the initial loading pressure at 25 °C was determined to be 62.65 psia. This maximum pressure was then used to determine the partial pressures of the constituent gasses for the hydrogen charging vessels.

$$PV = nRT \quad [1]$$

where:

P = absolute pressure of the gas,

V = volume of the vessel,

n = number of moles of gas,

R = ideal gas constant,

T = absolute temperature of the gas.

A hydrogen content of 1% was selected as the primary interest of this study, and 3% was included to assess the impacts of higher hydrogen contents while keeping the hydrogen content of the vessels below 4% to minimize concerns of flammability. Samples were also placed into vessels and loaded with pure argon to serve as an experimental control population and to further elucidate the effects of low temperature exposure on the test specimens. The vessels were stored at 100 and 200°C for seven and eleven weeks to assess if any impacts from varying exposure duration or temperature could be observed.

The gas composition of each hydrogen charging vessel was determined from pressure transducer measurements on the gas-mixing manifold used in their loading. In the case of mixed hydrogen and argon vessels, hydrogen was first added to the target pressure, followed by the addition of argon to obtain the desired final pressure. The difference in the total pressure and the initial hydrogen pressure was used to determine the partial pressure of argon added. The gaseous contents of the vessels used in this experiment are detailed in Table 2-1.

Table 2-1 Hydrogen Charging Vessels Initial Loading

Vessel Number	Nominal Atmosphere	H Pressure (mm Hg)	Ar Pressure (mm Hg)	Total Pressure (mm Hg)	Hydrogen Content (% total)
1	3% H in Ar	86.22	2765.47	2851.69	3.02%
2	1% H in Ar	28.91	2865.14	2894.05	1.00%
3	1% H in Ar	28.91	2865.14	2894.05	1.00%
4	1% H in Ar	29.05	2864.99	2894.04	1.00%
5	1% H in Ar	28.90	2865.12	2894.02	1.00%
6	Ar	0	2909.34	2909.34	0%
7	Ar	0	2903.81	2903.81	0%

The effect of surface roughness on hydrogen absorption behavior of Ti64 tensile specimens was investigated by testing samples in both the “as-printed” condition without any additional preparation, and the “machined” condition in which excess material was removed to provide a standard machined surface. Each vessel studied in this experiment contained tensile samples evenly split between the “as-printed” and “machined” conditions.

To further investigate the effect of printing variables, and in particular the effect of part elevation, samples printed with varying elevations above the build plate, as shown in Figure 2-1, were included in this study. These conditions were designated as being high (~ 25 mm above the BP), mid (~13 mm above the BP), and low (on or nearly on the BP).

Accounting for the build position and surface finish of the tensile samples, each vessel contained six samples, three in the “as-printed” condition and three in the “machined” condition with one sample from the high, mid, and low positions for each condition. The features of each sample (surface finish and build position) were readily identified by the sample identifier, which was printed into the top grip cross-sectional face. These identifiers served as a simple method of tracking samples and followed each specimen throughout the tests conducted.

The contents of an example vessel are shown in Table 2-2 The full sample list including sample conditions (sample identifier, build position, and surface finish) and the vessel number, and exposure conditions (environment, temperature, and duration) are listed in appendix A (Table 6-1).

Table 2-2 Example Hydrogen Exposure Vessel Contents and Conditions

Vessel Number	Exposure Atmosphere	Temperature (°C)	Duration (weeks)	Sample Identifier	Surface Finish	Build Position
1	3% H in Ar	200	7	D1	As-printed	High
1	3% H in Ar	200	7	D2	Machined	High
1	3% H in Ar	200	7	D3	As-printed	Mid
1	3% H in Ar	200	7	D4	Machined	Mid
1	3% H in Ar	200	7	D5	As-printed	Low
1	3% H in Ar	200	7	D6	Machined	Low

2.4 Mechanical Properties Testing

Mechanical properties of the exposed samples were investigated using tensile testing conducted on a MTS Criterion Model 43 system (MTS Inc.) equipped with a 50 kN load cell. Load and crosshead data were captured using the MTS control software and exported using the accompanying MTS TestSuite TW Elite software. The tensile tests were conducted at a crosshead speed of 0.255 cm/min and testing was conducted consistent with ASTM E8. A wedge type grip was used to hold the samples.

Digital image correlation (DIC) was used to calculate contactless strain measurements and generate strain maps of the test specimen during the tensile tests. DIC was conducted using a VIC-3D 8 system (Correlated Solutions Inc.) with two 12.3-megapixel cameras. DIC data acquisition used the VIC SNAP 9 interface and data was processed with the VIC-3D 8 software packages. Images were acquired at a rate of 4 Hz, and the cameras focus was calibrated using a NIST-traceable calibration grid.

Samples were prepared for DIC analysis by applying a random black and white “speckle” paint pattern as shown in Figure 2-3. This random pattern provides a method of contrast by which the DIC software analyzes the change in the grey value across a series of subset areas in each picture. The change in grey value across each subset is tracked between each image, and is translated to material dislocation and in turn, strain by the software. An example strain map generated by the DIC software is shown in Figure 2-4.

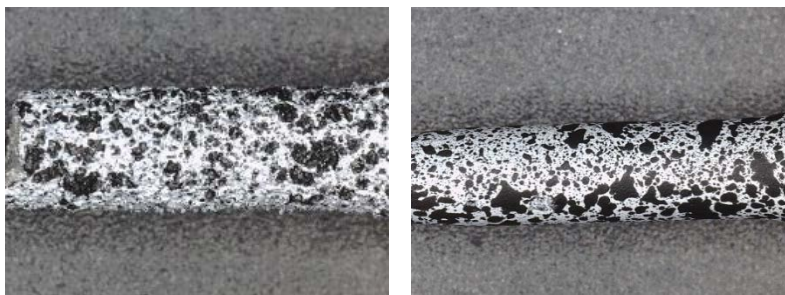


Figure 2-3 Photos of example speckle patterns applied to tensile specimens in the as-printed condition (left) and as machined (right).

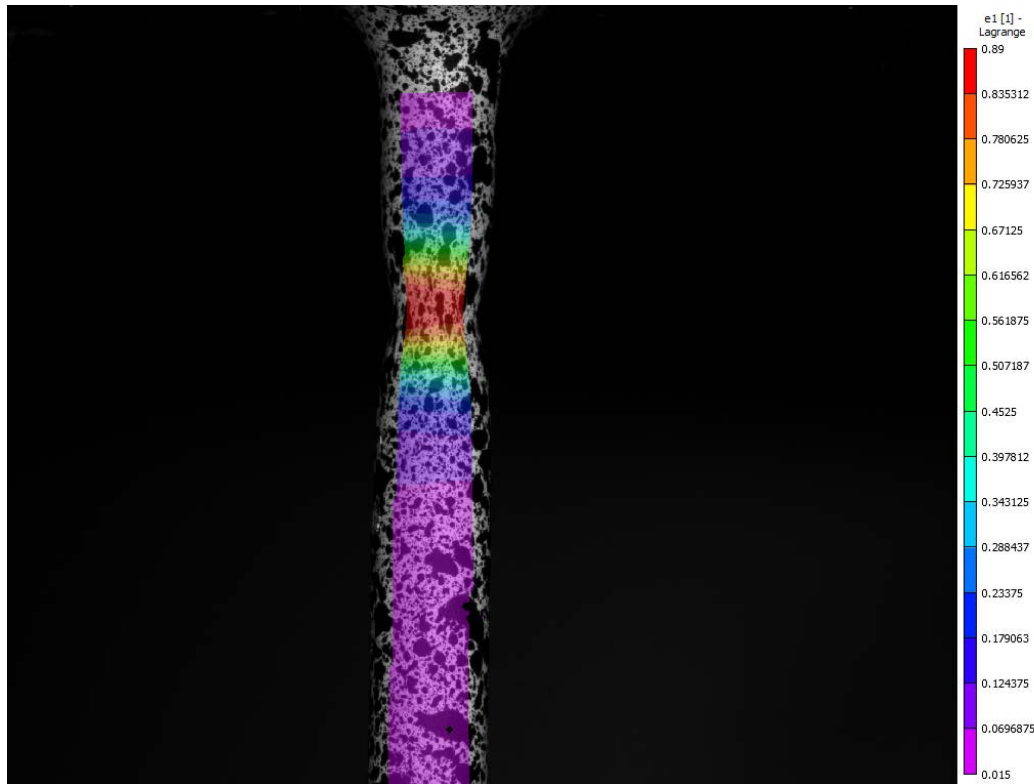


Figure 2-4 Example strain map of a tensile specimen generated using digital image correlation.

2.5 Fractography

Tensile test samples were examined on a Keyence VR3000 3D macroscope to evaluate the fracture samples and the fracture surface. In addition, selected tensile samples were examined on a Hitachi Scanning Electron Microscope (SEM). The higher magnifications of the SEM enable one to determine the fracture micromechanisms.

2.6 PVT testing

PVT testing, to determine the hydrogen uptake characteristics of the AM Ti64, was conducted by Hydrogen Isotopes Processing Science Group (HIPS). AM cylinders that would fit into the standard test cell were machined from the AM tensile samples. The sample was placed in the sample cell and was attached to a SS stand-off tube using a ¼" 4VCR ½ micron filter gasket which in turn was connected to a Swagelok valve. That valve was connected to a SS ¼" 4VCR tee. One branch of the tee had a Paroscientific pressure transducer mounted on it, while the third branch connected to a second Swagelok valve. The entire assembly, called the 'test cell' was attached to the HIPS Manual Manifold, a SS Sieverts' apparatus, for the experiments. The vacuum integrity of the assembly was always confirmed after installation.

A total of 5 samples were studied to date under slightly differing protocols designed to determine when a treated or untreated rod would begin to absorb research grade hydrogen (H_2). The samples were designated Ti64_#, where the integer '#' ranged from 1 to 5. The protocols used and the results obtained are described below. Initial and final sample weights are shown in Table 2-3. The differences observed there are essentially within the experimental error and probably do not reflect the hydrogenation extent.

Table 2-3. Sample weights before and after processing and sample condition tested

ID	Initial Wt (g)	Final Wt (g)	Est. H/M	Condition
1	1.794	1.795	.0053	As-Machined
2	1.807	1.806	.0056	As-Machined
3	1.838	1.838	.0051	As-Machined
4	1.823	1.820	.0045	Abraded
5	1.768	1.771	.046	Thermally Activated

All samples were passivated before removing from the sample cell. This consisted of a three-fold repetition of: evacuating the sample, closing the sample cell valve, adding air to the main manifold, expanding the air into the sample cell, and watching for indication of reaction (excess pressure drop, sample temperature rise). No reaction was ever observed. After passivation the sample was removed from the cell and placed in a sample holder for subsequent analysis.

Initially, cell volumes were calibrated with normal procedures which consisted of either research grade bottled He or house Ar (Ar liquid boil-off) expansion step-wise into the sample cell. Because of the possibility that the Ar contained trace oxygen which potentially could passivate the rod surface, research grade He was used in some cases. In the end this did not seem to be relevant. In addition in a couple of cases, the Ar/He filled cell was heated to higher temperatures and the pressure changes monitored in order to attempt to use the ‘apparent volume’ change (which arises since the manifold remains at room temperature while the cell is heated) to monitor hydrogenation. However, this approach was subsequently found to not work, probably due to slow heat transfer from the heater, which surrounds the sample cell like an oven, to the actual rod in the sample cell. (Some data regarding this shown below.) Typically, the volumes obtained were: sample cell – 11.24 cc (at room temperature), tee assembly (‘between the valves’) – 6.66 cc, manifold connection – 4.63 cc or 2.73 cc. (Sample #1 was initially connected to the 4.63 cc connection and later moved to the 2.73 cc one. The rest of the samples were connected to the 2.73 cc point). The manifold volume was 51.645 cc when the 4.63 cc connection was used, otherwise it was 45.619 cc. Heating the sample to 450-460 °C typically increases the pressure, which is compensated for by the apparent volume technique, which gives an ~2 cc apparent volume decrease for the higher temperature test cell volume.

3.0 Results

3.1 Printed Objects

A number of different objects were printed for this project, including training articles, tooling, prototypic objects, and test pieces. A few of these are shown in Figure 3-1. These valves show the support material that was not easily removed during post-processing. Simulated training reservoirs are also shown, to demonstrate that a level of fidelity for training is readily achieved. Tensile and microstructure blocks are also shown. These samples can be processed from the base plate up or can start above the baseplate provided some heat source material is printed in the sintered powder. This feature is different than what is possible for L-PBF systems, which require material be deposited on the baseplate.

Not all print jobs are successful and Figure 3-2 shows a simulated reservoir print that failed due to swelling caused by an excessive amount of melting. The job was restarted, and the job continued from where it failed rather than at the beginning of the job, as might have been expected.

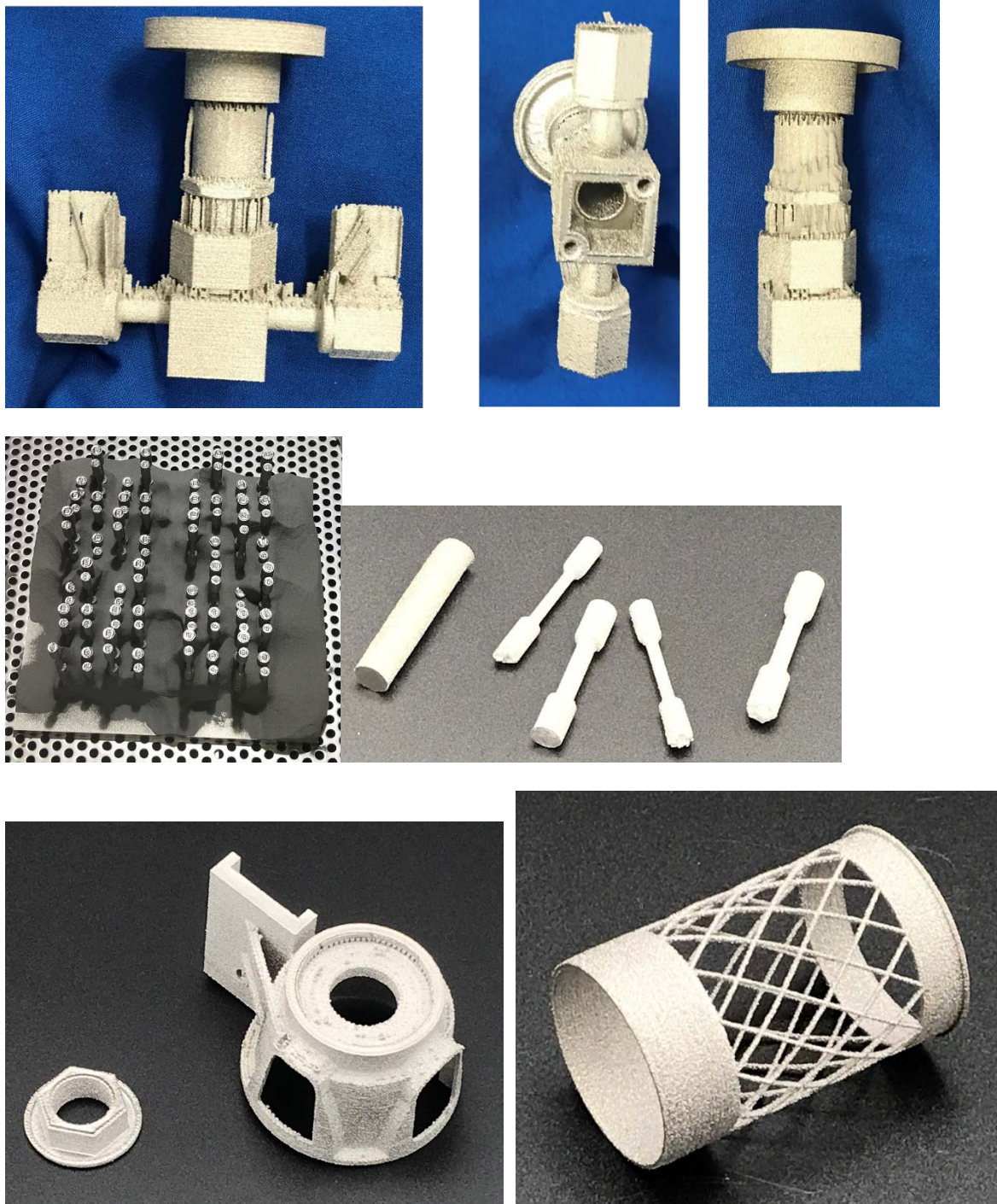


Figure 3-1 Simulated valves, tensile samples on the build plate and separated from it in the as-printed condition, a Dremel too stem cut-off holder, and a light weight fuel cell holder article.

3.2 Metallography

Cross-sections of tensile samples are shown in a number of different conditions. The baseline microstructure of AM Ti64 can be comprised of widmanstatten martensite, a lamellar structure with acicular alpha', or a lamellar structure of alpha and beta phases. The plate like structures consist of alternating layers of light colored alpha and darker appearing beta phases. In addition to these phases, a nearly continuous beta grain is present parallel to the print direction. This phase occurs because of a combination of the solidification rate, thermal gradient, and partitioning factors for the elements that comprise Ti64.

The typical as fabricated microstructure in the longitudinal orientation is shown in Figure 3-3. The large beta grains are visible in the lowest magnification image and slightly off parallel with the edge of the sample. The surface roughness is also visible in this image. The layer by layer fabrication method can be inferred from the microscopy as well. Small pores are apparent in the center image and based on the shape, these are likely lack of fusion defects. The spherical pore in the image on the right could be due to gas porosity in the starting powder or from keyhole porosity caused by the electron beam interactions with the powders.

The typical as-fabricated microstructure from a transverse cross-section of a tensile bar is shown in Figure 3-4. The surface roughness is apparent at the low magnification images. The presence of fine porosity is apparent. The alpha and beta layered structure is visible at the highest magnifications. The individual colonies of the lamella typically initiate growth from the beta phases.

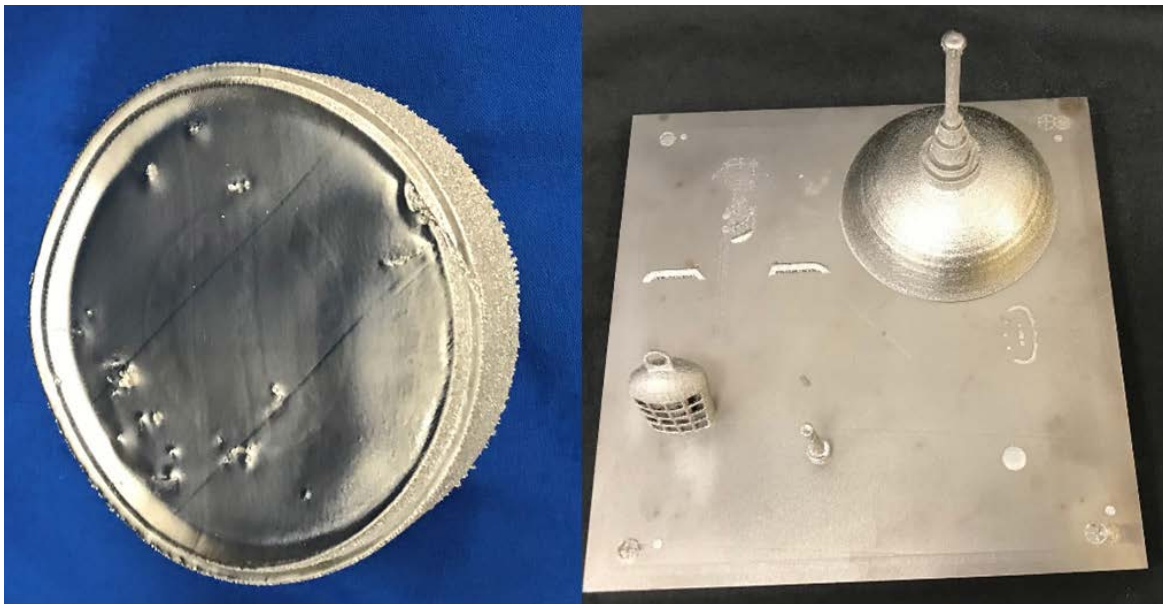


Figure 3-2 This image shows a print job that was interrupted / failed due to swelling, the job was continued from the stop point rather than restarting the job.

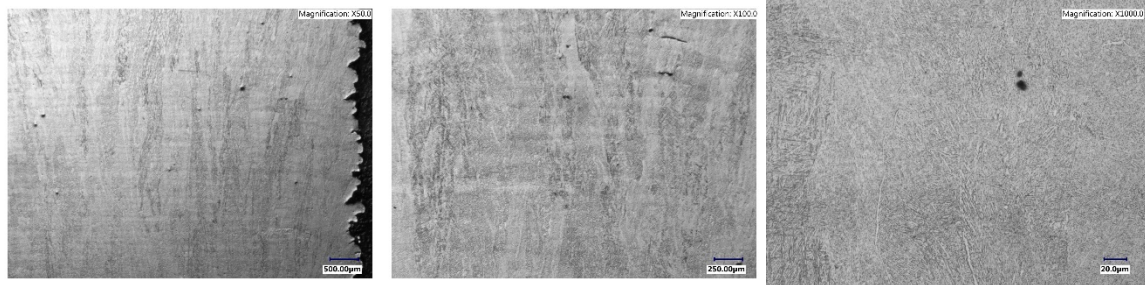


Figure 3-3 Longitudinal section of showing the extended beta grains from low to high magnification

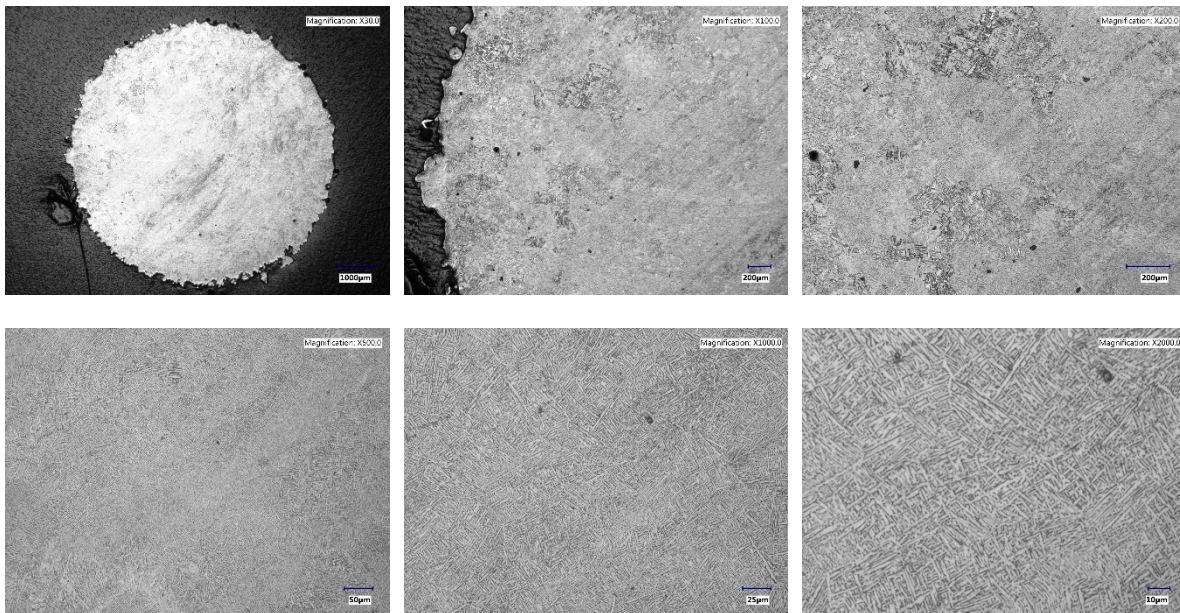


Figure 3-4 Transverse cross-section of as-fabricated Ti64.

3.3 Hydrogen Charging

Metallographic cross-sections after aging in argon at 200°C for six weeks for the transverse orientation are shown in Figure 3-5. There was no increase in the alpha case for the low temperature, low argon exposure. No obvious changes were visible in the longitudinal orientation either, Figure 3-6

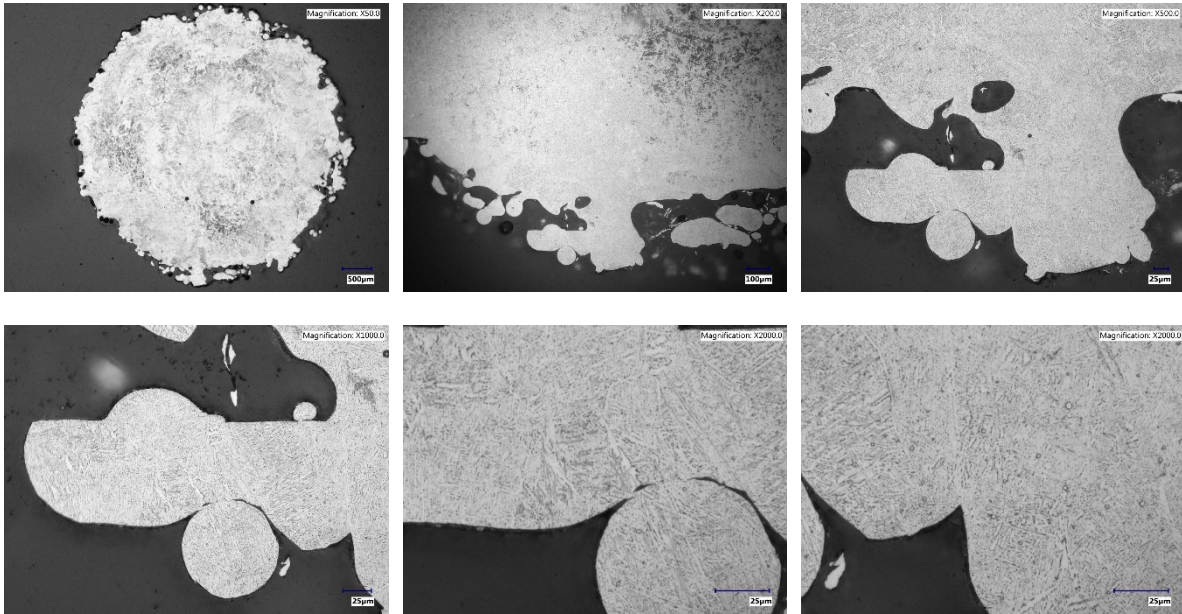


Figure 3-5 Transverse cross-sections showing the lack of alpha phase formation for an Ar exposed sample.



Figure 3-6 Longitudinal cross-section of an Ar exposed Ti64 sample.

Similar metallographic examination was conducted after the hydrogen exposure, Figure 3-7. The examination of these samples was also concentrated on the surface features since hydriding is expected to initiate on the surface and progress inwards. No hydrides are observed. One interesting feature is the lack of microstructural features on the particle. It is possible that this particle was trapped and is not bonded to the surface and has not undergone the melting and solidification process. This particle may have too fine a microstructure to be resolved.

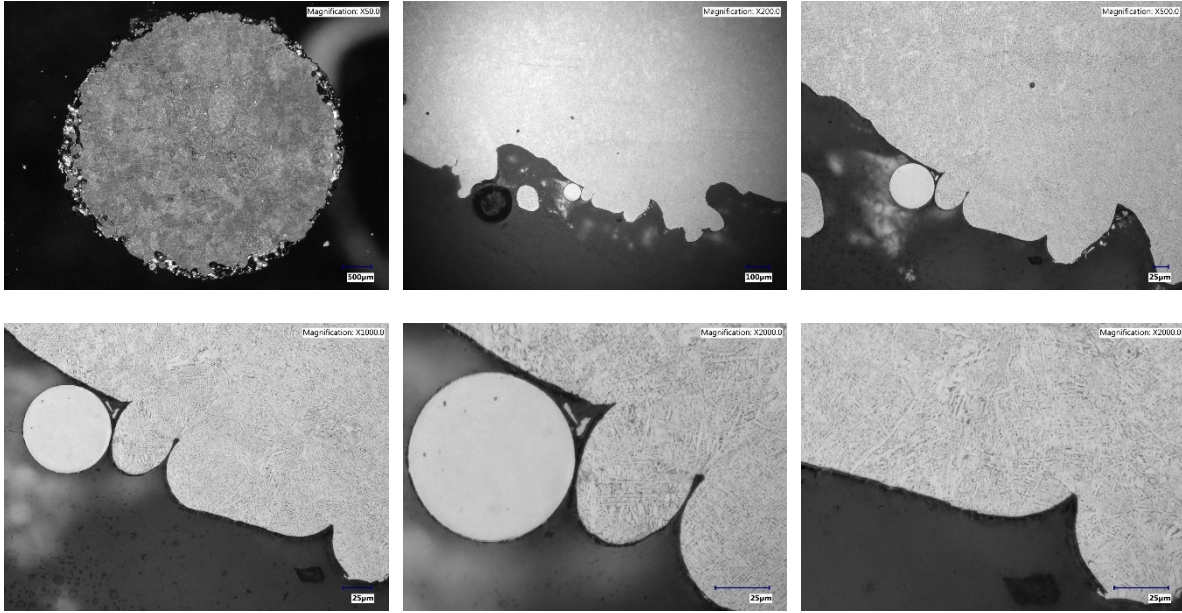


Figure 3-7 Transverse sample metallography after hydrogen exposure at 200C for 6 weeks showing the lack the hydride formation.

A longitudinal cross-section after hydrogen exposure is shown in Figure 3-8. No microstructure changes are apparent. There are no indications that hydrides formed on the surface of the sample, hydrides would be present as needle like phases that would likely be parallel to the alpha / beta interfaces.

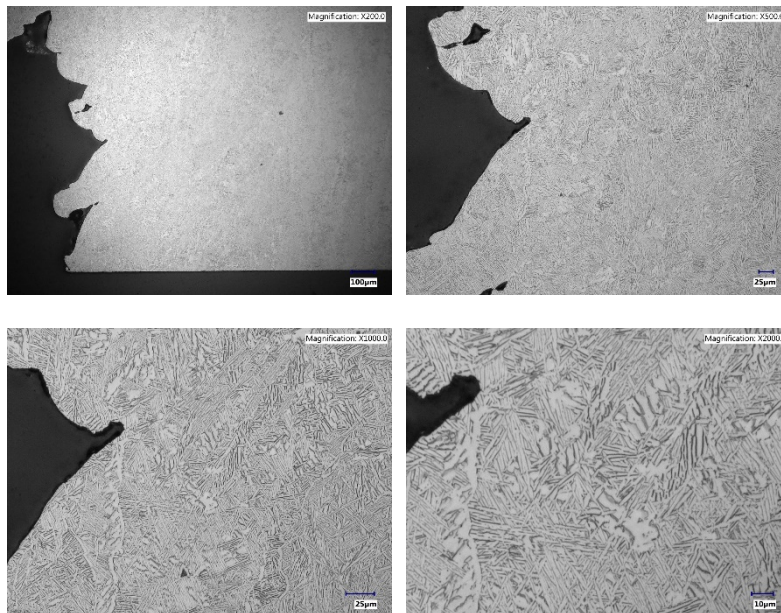


Figure 3-8 Longitudinal cross-section of a sample exposed to hydrogen for six weeks at 200°C.

3.4 Mechanical Properties

Mechanical property testing of the hydrogen and argon exposed samples suggests that no discernable effects were observed as the result of these low temperature exposures. A greater difference in performance

between the specimens can be attributed to the surface roughness of each sample, either as-printed or machined. The effects of which are discussed in greater detail below. Individual test data are presented in Appendix A (Figure 6-1 through Figure 6-7).

This lack of hydrogen-induced embrittlement agrees with the absence of hydrides observed during metallographic examination of the hydrogen-exposed specimens. The effects of temperature, up to 200 °C, and hydrogen content, up to 3% hydrogen in argon, were indiscernible in the tensile performance of the specimens studied as shown in Figure 3-9.

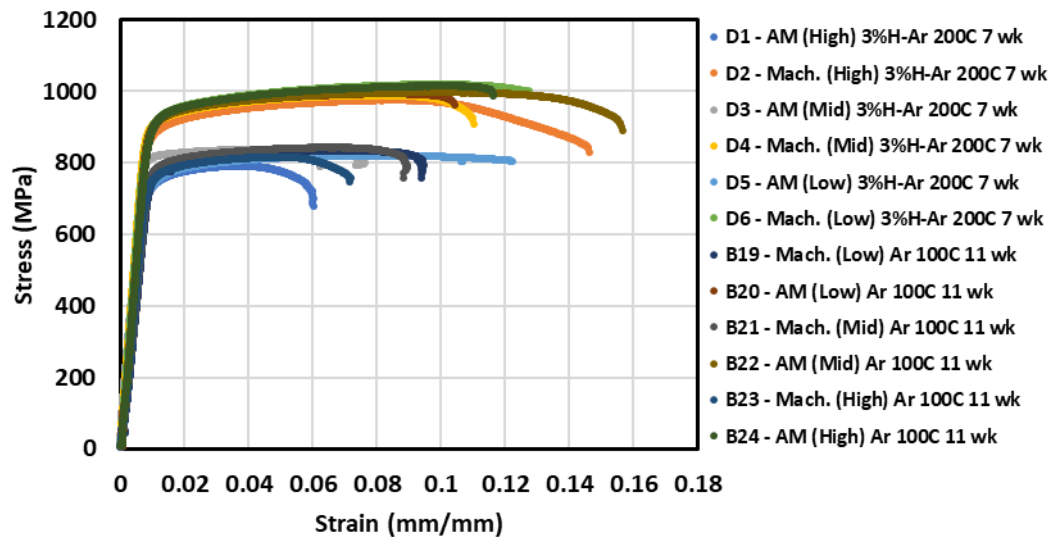


Figure 3-9 Tensile property comparison of samples exposed to 3% hydrogen in argon at 200 °C for 7 weeks and argon at 100 °C for 11 weeks

Further comparison of tensile performance in samples exposed to 1% and 3% hydrogen atmospheres as displayed in Figure 3-10, demonstrates a similar lack of effect between the exposure conditions.

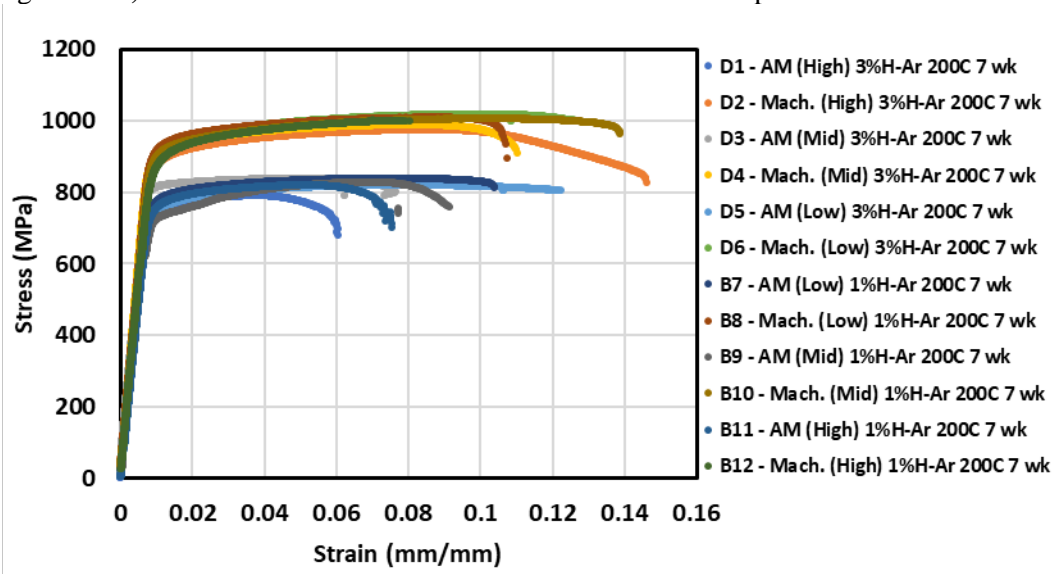


Figure 3-10 Tensile property comparison of samples exposed to 3% and 1% hydrogen environments at 200 °C for 7 weeks.

While it was initially hypothesized that higher temperature exposure may promote hydrogen absorption and mechanical property degradation, exposure to temperatures up to 200 °C do not appear to degrade the mechanical properties or induce hydriding in the low hydrogen atmospheres studied.

A decreased yield stress is observed in the as-printed samples after the 100 °C exposure, as shown in Figure 3-11. However, due to the lack similar effect at higher temperatures, this may be the result of a sampling effect induced by localized print variation or a measurement effect.

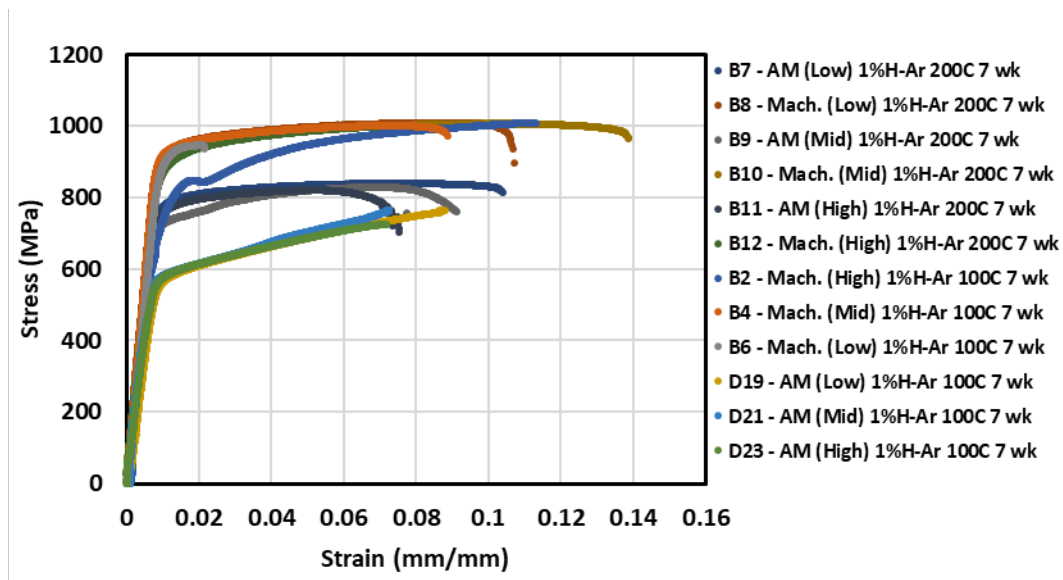


Figure 3-11 Tensile property comparison of samples exposed to 1% hydrogen in argon at 100 °C and 200 °C for 7 weeks.

The most significant effect observed during the mechanical properties testing was attributed to the surface finish of the specimens. In comparing the performance of as-printed samples to those having undergone machining, resulting in reduced surface roughness, machine-finished samples displayed a consistent improvement in both strain to failure and the ultimate stress over as-printed samples. The reduction in yield and ultimate tensile strengths for the as-printed condition can be attributed to including some partially densified material on the surface of the specimens as indicated in Figure 3-7

No differences to hydrogen exposure were observed between the as-printed and machined samples. Despite the initial hypothesis that the as-printed surfaces would be more susceptible to hydriding due to the increased surface area of as-printed surface, no effects were observed up to 200 °C for environments containing up to 3% hydrogen.

While the difference in machined and as-printed samples is apparent from many of the tests, this effect may be further isolated by comparing specimens at a single build height, as shown in Figure 3-12 in which samples of a fixed build elevation display a similar improvement in tensile performance moving from as-printed to a machined surface after varying exposure conditions.

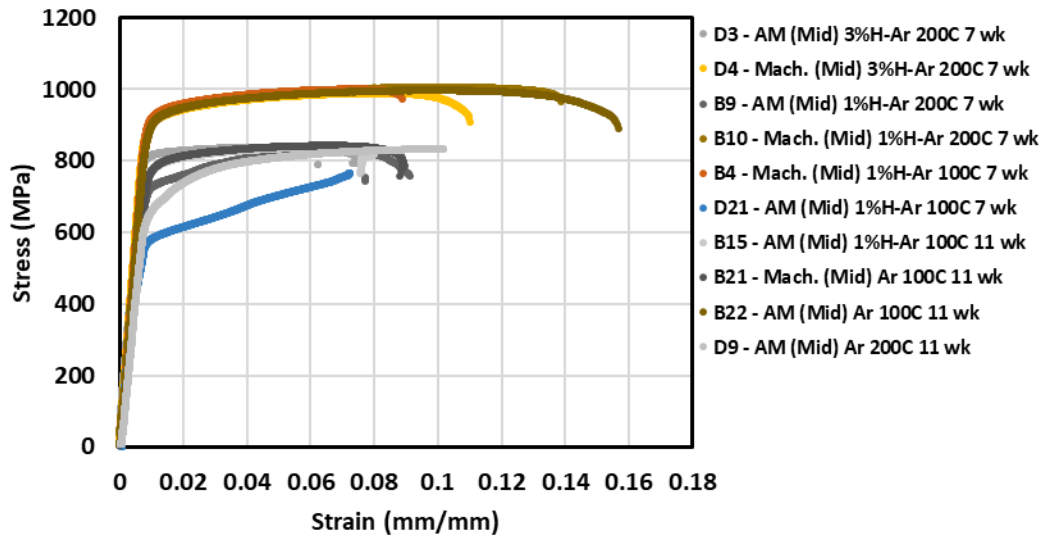


Figure 3-12 Tensile property comparison of samples printed at the “middle” build position under varying exposure conditions.

The observed effect on mechanical properties most likely results from the roughness of the as-printed surfaces, which facilitate crack initiation during failure, whereas the machined samples tended to display more uniform elongation prior to necking and failure. This finding is supported by low magnification optical fractography conducted on tensile specimens. Samples in the as-printed condition more frequently displayed little necking and an angled fracture, as shown in Figure 3-13. By comparison, samples with machined surfaces tended to exhibit necking and fracture perpendicular to the stress axis as displayed in Figure 3-14.

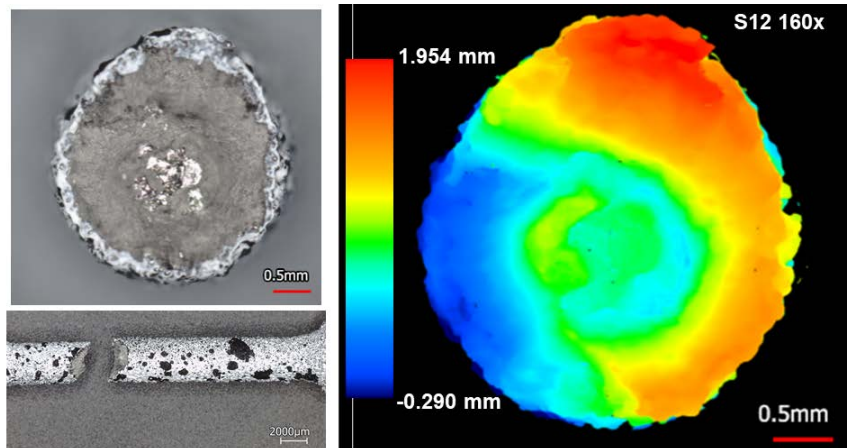


Figure 3-13 Low-magnification fractography of a tensile specimen in the as-printed condition

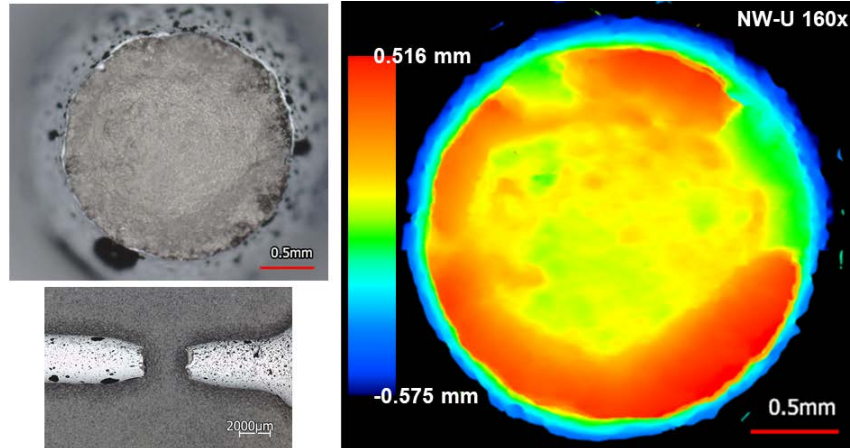


Figure 3-14 Low-magnification fractography of a tensile specimen in the machine-printed condition

The final effect on tensile properties considered is the location of the tensile specimen on the 3D printer build plate. This placement resulted in variation in the strain to failure, with no discernable impact on the ultimate stress in both the as-printed and machined samples. However, no consistent trends were identified among the three build heights examined, suggesting that additional data on printing conditions are necessary to characterize the build position and the mechanical properties. Ultimately, the variation observed as the result of printing height off the build plate exceeded the changes in mechanical properties induced by hydrogen exposure.

3.4.1 SEM fractography

SEM Fractography was conducted on the D-series samples that were from the low, medium, and high locations in the as-printed and machined conditions after exposure to 3% H in Ar at 200 °C for 7 weeks. There are differences in the macrofailure appearance between the as printed Figure 3-15 and machined samples Figure 3-16 for samples at the high position, but examination of the fracture surface at high magnification, doesn't exhibit any noticeable differences.

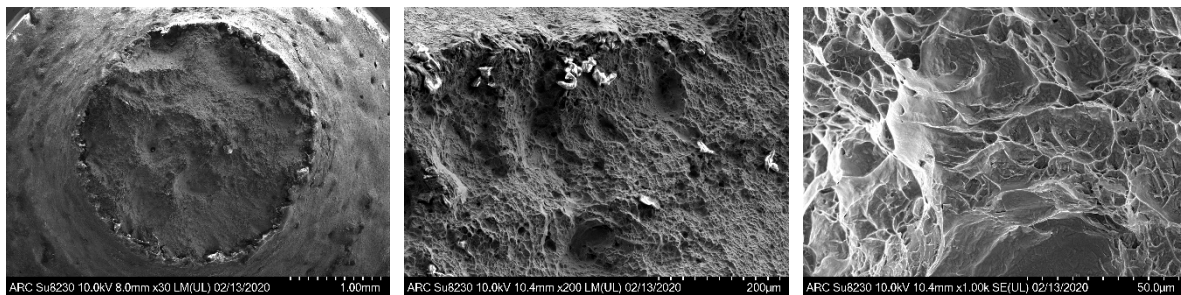


Figure 3-15 Sample D1, as printed from the high position, after exposure at 3% H₂ at 200 C for 7 weeks.

The samples from the low position are also consistent between the as-printed, Figure 3-17, and machined surfaces, Figure 3-18. There are differences in the size of the voids with the high sample having larger voids, Figure 3-15, compared to the low elevation sample, Figure 3-17 for the as printed samples.

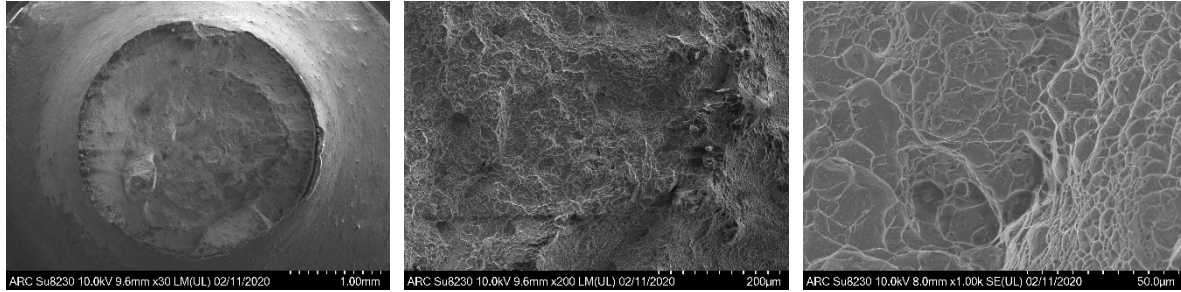


Figure 3-16 Sample D2, machined from the high position, after exposure to 3% H₂ at 200 °C for 7 weeks.

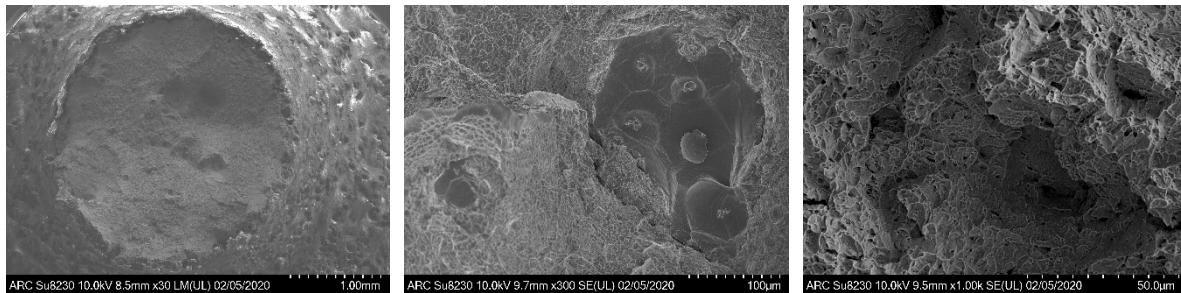


Figure 3-17 Sample D5, as-printed from low position, after exposure to 3% H₂ at 200 °C for 7 weeks.

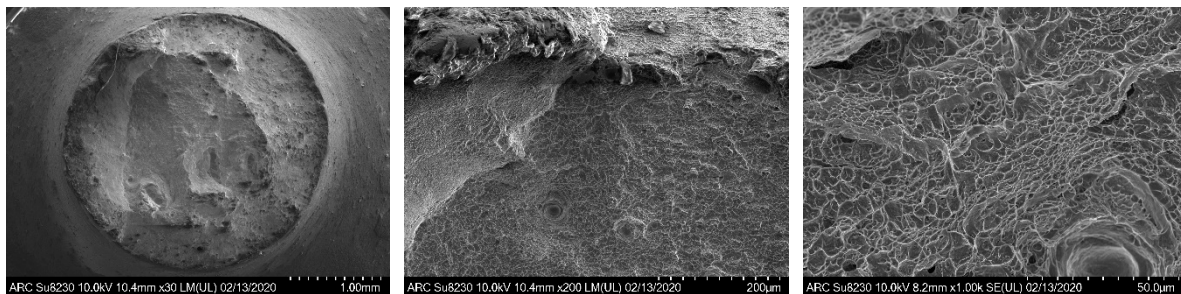


Figure 3-18 Sample D6, machined sample from low position, after exposure at 3% H₂ at 200 °C for 7 weeks.

3.5 PVT Testing

The results from the five samples tested for hydrogen absorption are described below.

3.5.1 *Ti64_1*

The first sample was volume calibrated at room temperature three times with He. A brief heater pulse was applied to the evacuated cell to test heater function and subsequently ~ 86 Torr of H₂ was added to the cell while it was at a low temperature (~70-80°C). The sample cell was then heated. Figure 3-19 shows the sample temperature (T) and cell pressure (P) obtained versus elapsed time. As the sample warms, the

apparent volume decreases, i.e. the pressure increases without absorption. The sample was warmed to $\sim 150^{\circ}\text{C}$ and held there briefly. Then manual set point increases were started while watching for evidence of absorption. The typical changes were about $+10^{\circ}\text{C}$ every 3 minutes.

At about 106 torr it was noted that the pressure seemed to be increasing too fast for the ramp, so the temperature was held at $\sim 380^{\circ}\text{C}$ for a short time (flat part of curve at $\sim 2.75\text{-}3$ hr). This showed that absorption was not occurring so set point increases were resumed up to 450°C and held there. Pressure peaked at 156 torr at 4.5 hr, then began decreasing. The heater was turned off at the end of the day (i.e., the end of the data record) at ~ 8.25 hr, where P had decreased to 17.9 Torr at 450°C (from the peak of ~ 156 Torr).

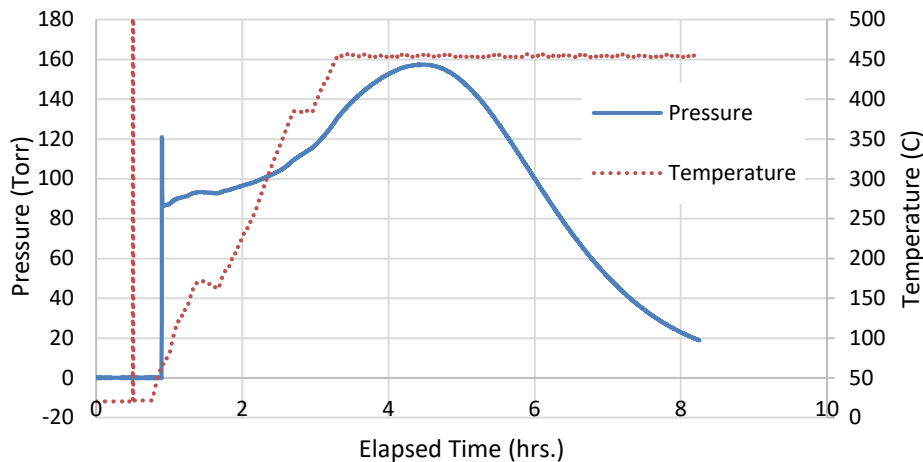


Figure 3-19 Raw data for hydriding sample Ti64_1

Figure 3-20 presents the pressure and temperature relationship for the warming period. Note that P is not constant at constant sample T of ~ 380 and $\sim 450^{\circ}\text{C}$. This implies either big lag effects or desorption of some unknown species, therefore we probably can't interpret dynamic experiments as initially thought (with 'apparent volume'). It is unclear why P increases while at constant T. Gas evolution of some sort would cause this, but the specific identity of the gas would require mass spectral analysis, which was not attempted. Alternatively, because the physical contact between the sample rod and the sample cell is probably limited to the bottom of the rod and the point where the rod leans against the sample cell, lag between recorded T and actual T could be appreciable due to poor heat transfer rates.

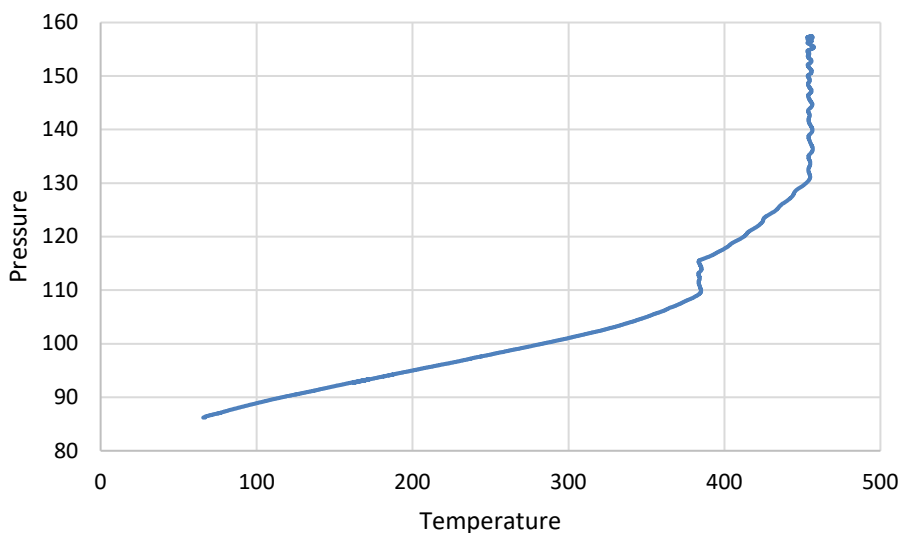


Figure 3-20 Pressure vs. sample temperature during heating (Ti64_1)

Once the sample cell had cooled back down to room temperature, pressure measurements indicated that the H/M value obtained for this reaction was in the vicinity of 0.004 (uses a calculated AMU = 46.7369 grams alloy/mole M).

This sample was evacuated and Ar added in order to examine apparent volume changes with temperature. Due to the observations noted in Figure 3-20, this data will not be considered further. After those experiments the sample was re-exposed to H₂ and the temperature raised to 450°C again, but no further absorption was noted after a ~1/2 hour hold at temperature. The sample was then cooled, evacuated, passivated, and dismantled.

3.5.2 Ti64_2

This sample was inserted into the cell, evacuated, and volume calibrated with Ar at room temperature three times, followed by one calibration with He. Subsequently, while still under He, the sample was heated up and run for ~1 hour for a short temperature excursion before being cooled down. On the following day more temperature ramp experiments with He were conducted that will not be analyzed here.

Once the temperature had reached ~200°C, the He was evacuated and H₂ added, but no absorption was noted at that point. The heater set point was then slowly increased (step-wise) up to ~265°C with no indication of absorption, whereupon the sample was cooled off. Pressure measurements the next day confirmed a lack of absorption. The sample was heated back to ~250°C and the slow set point increases continued. The temperature was slowly increased to ~340°C with no indication of absorption. The sample was left at temperature for ~87 hours with no indication of absorption. The sample temperature was then heated up to ~410-420°C and absorption was noted at that point. The sample was held there for ~4 hours and then cooled. Figure 3-21 shows the time plots of pressure and temperature for this run. The sample was then evacuated, passivated, and removed.

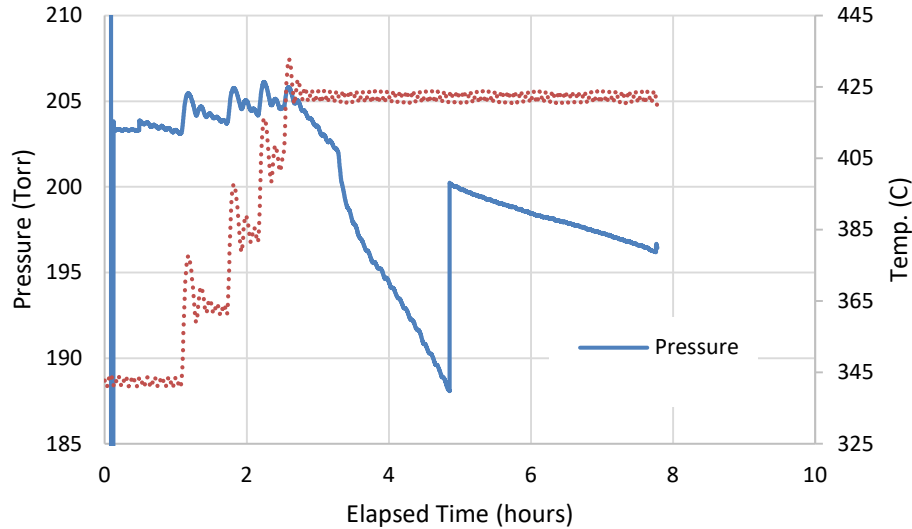


Figure 3-21 PVT testing form sample Ti64_2

Of note in Figure 3-21 is the apparent drop in pressure starting at ~2.6 hours. However careful examination shows that the pressure trace shows similar slight decreases after each temperature excursion when the set point had been increased. The drop at 410-420°C was potentially due to the same effect, however, that also was the temperature at which absorption was expected to commence. Therefore (since the time period was over the lunch period), it was held at that point. At ~3.3 hours, there was a more significant drop observed, which subsequently slowed somewhat but continued at the slower rate.

3.5.3 Ti64_3

The sample was evacuated, and volume calibrated at room temperature with He two times. Subsequently, hydrogen was added, and the sample heated up to ~310°C with no absorption, whereupon it was cooled back to room temperature. The next day it was heated to ~440°C and slow absorption noted during a 4 hour hold at temperature. The time plots of the two pressure sensors and the sample temperature are shown in Figure 3-22. Of note is the drop at ~440°C, but also the non-flat period in the pressure traces at ~1-1.8 hours versus the subsequent response to set point changes. It is unknown why that occurred. The jump in P at the end is due to closing the test cell valve. The sample was later evacuated, passivated, and dismantled.

3.5.4 Ti64_4

Prior to inserting this sample in the sample cell, it was abraded briefly with 600 grit paper. It was then placed in the sample cell and mounted and evacuated as fast as possible (probably 2-3 minutes from the end of abrasion to vacuum). H₂ was then added and the sample heated to 220°C with no apparent absorption, after which it was cooled. The next day, heating was resumed, and at ~365°C absorption was observed. The sample was held there for ~5.5 hours and cooled (see Figure 3-23). Subsequently it was evacuated, passivated, and dismantled.

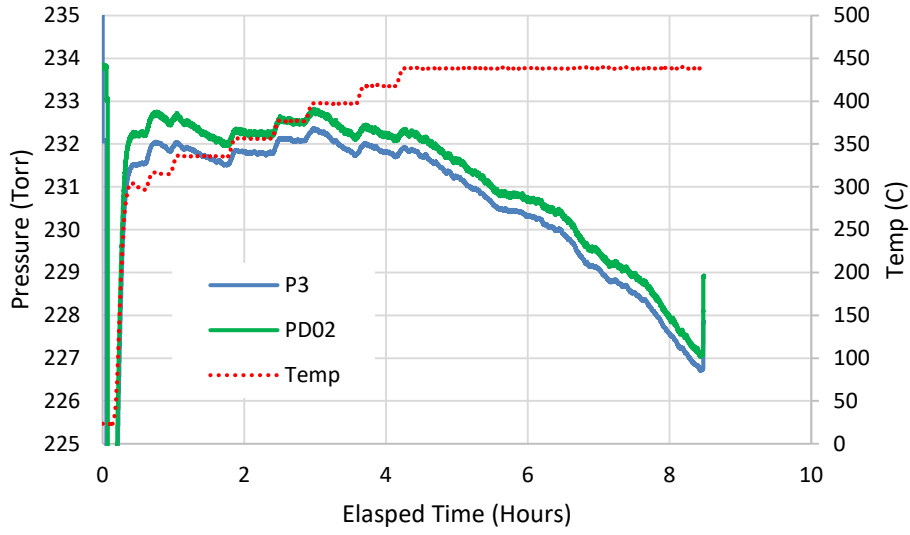


Figure 3-22 Ti64_3 Hydridding occurred after heating to over 400°C.

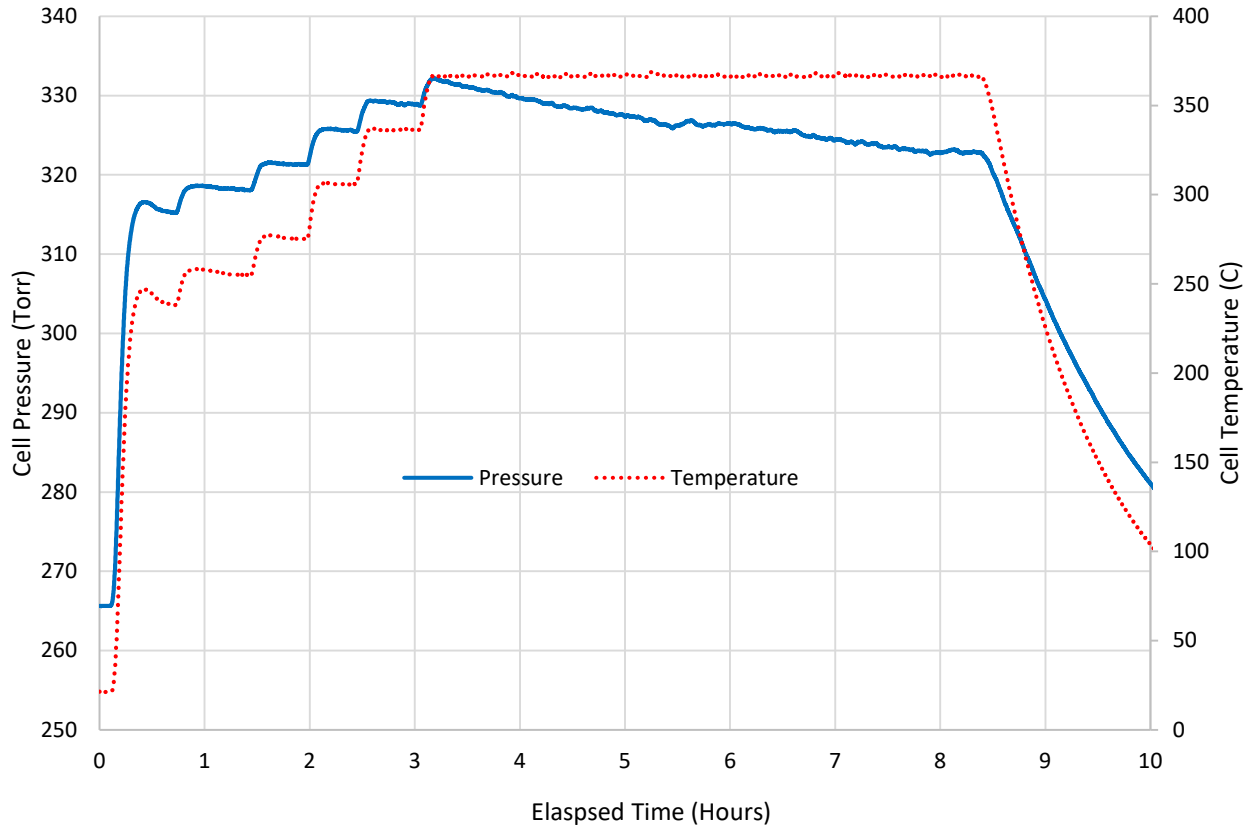


Figure 3-23 Pressure and temperature plot for the sample Ti64_4 showing hydridding at lower temperatures than with machined surfaces.

3.5.5 Ti64_5

This sample was pretreated by heating under vacuum to 550°C and holding there for ~1 hour. After cooling back to room temperature, hydrogen was added, and the sample was heated to ~250°C. The sample immediately began absorbing hydrogen, so it was held at that temperature for ~6.5 hours (see Figure 3-24). It was then cooled, evacuated, passivated, and dismantled.

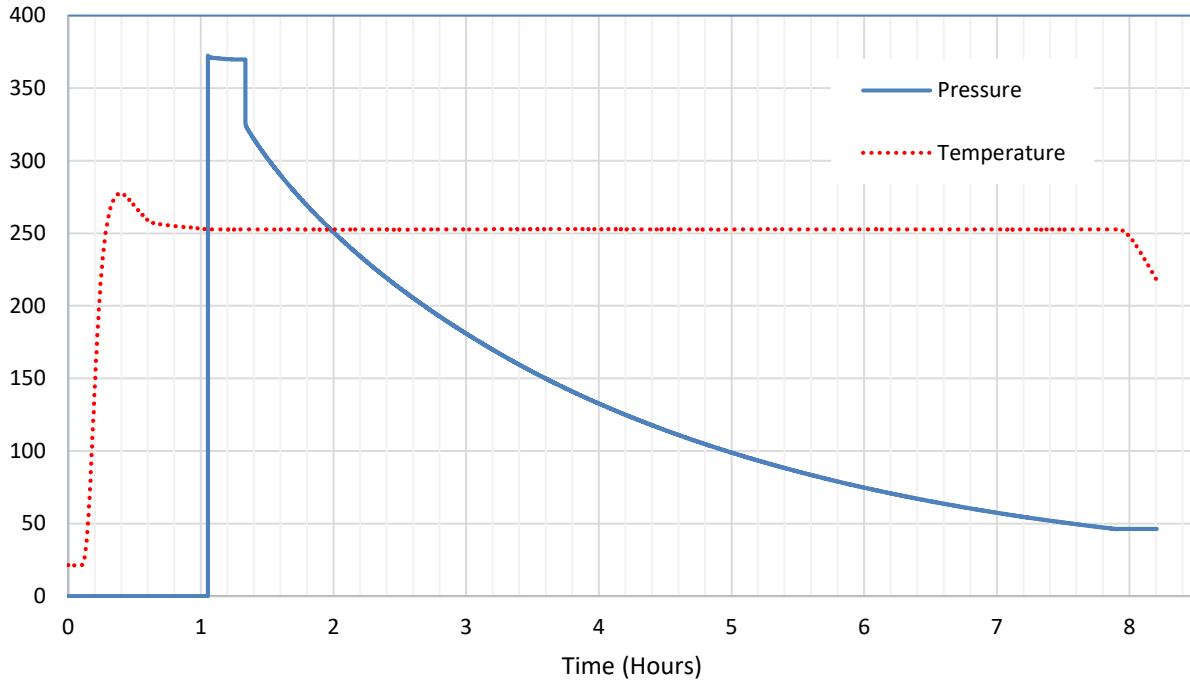


Figure 3-24 Preheating samples to activate the surface results in hydriding at significantly lower temperatures.

The results from the five samples tested for hydrogen absorption, including the onset temperatures of hydriding are summarized below in Figure 3-24.

Table 3-1 Hydride on-set temperature for hydriding

ID	Sample Condition	Onset Temperature (°C)
Ti64_1	As-Machined	450
Ti64_2	As-Machined	410
Ti64_3	As-Machined	440
Ti64_4	Abraded	367
Ti64_5	Thermally Activated	250

4.0 Conclusions

The Arcam A2X successfully printed test components and tooling in Ti-6Al-4V. Components and prototypes were consistent with the target geometry that were desired.

The standard printing parameters produced nearly fully dense structures. There were some random pores and a minimum of lack of fusion defects.

Post hydrogen exposure at temperatures up to 200°C for 2 weeks did not result in hydride formation based on the mechanical properties or metallographic examination. Samples were examined in the as-fabricated and machined conditions with no evidence of hydride observed metallographically.

The mechanical properties varied significantly more based on elevation above the build plate compared to the presence or absence of hydrogen.

Hydrogen exposure testing revealed the importance of sample surface preparation. As-machined surfaces did not absorb hydrogen until the temperature exceeded 400°C. An abraded surface started absorbing at 350°C. While a vacuum treated / activated surface absorbs at 250°C.

5.0 Recommendations, Path Forward or Future Work

The results reported to date indicate that the as fabricated and natural oxide film inhibit the rapid uptake of hydrogen. A tritium exposure at low levels would show if an as-fabricated or surface machined AM part could be used for glovebox usage with incidental tritium exposure.

Alternative alloys that are inherently more hydrogen / tritium resistant should be evaluated.

The methodologies developed here for hydrogen compatibility of the AM components should be utilized to determine the efficacy of use for incidental hydrogen isotope exposure while more invasive / higher hydrogen and tritium exposure conditions should be used for gas wetted applications.

6.0 References

P. Pinke, L. Caplovic, & T. Kovacs, https://www.kfki.hu/~anyag/tartalom/2007/oktober/Pinke_2.pdf, Sept. 2020

B. Gaspar, <https://pdfs.semanticscholar.org/a980/c7b07f82bbda605e91e562e9ae5391315b53.pdf>, Sept. 2020

ASTM E8 / E8M-16ae1, Standard Test Methods for Tension Testing of Metallic Materials, ASTM International, West Conshohocken, PA, 2016, www.astm.org

Appendix A. Detailed Results Hydrogen Charging and Tensile Testing

Table 6-1 Hydrogen Exposure Vessel Contents and Conditions

Vessel Number	Exposure Atmosphere	Temperature (°C)	Duration (weeks)	Sample Identifier	Surface Finish	Build Position
1	3% H in Ar	200	7	D1	As-printed	High
1	3% H in Ar	200	7	D2	Machined	High
1	3% H in Ar	200	7	D3	As-printed	Mid
1	3% H in Ar	200	7	D4	Machined	Mid
1	3% H in Ar	200	7	D5	As-printed	Low
1	3% H in Ar	200	7	D6	Machined	Low
2	1% H in Ar	200	7	B7	As-printed	Low
2	1% H in Ar	200	7	B8	Machined	Low
2	1% H in Ar	200	7	B9	As-printed	Mid
2	1% H in Ar	200	7	B10	Machined	Mid
2	1% H in Ar	200	7	B11	As-printed	High
2	1% H in Ar	200	7	B12	Machined	High
3	1% H in Ar	200	11	D13	As-printed	High
3	1% H in Ar	200	11	D14	Machined	High
3	1% H in Ar	200	11	D15	As-printed	Mid
3	1% H in Ar	200	11	D16	Machined	Mid
3	1% H in Ar	200	11	D17	As-printed	Low
3	1% H in Ar	200	11	D18	Machined	Low
4	1% H in Ar	100	7	B2	Machined	High
4	1% H in Ar	100	7	B4	Machined	Mid
4	1% H in Ar	100	7	B6	Machined	Low
4	1% H in Ar	100	7	D19	As-printed	Low
4	1% H in Ar	100	7	D21	As-printed	Mid
4	1% H in Ar	100	7	D23	As-printed	High
5	1% H in Ar	100	11	B13	As-printed	High
5	1% H in Ar	100	11	B14	Machined	High
5	1% H in Ar	100	11	B15	As-printed	Mid
5	1% H in Ar	100	11	B16	Machined	Mid
5	1% H in Ar	100	11	B17	As-printed	Low
5	1% H in Ar	100	11	B18	Machined	Low
6	Ar	100	11	B19	As-printed	Low
6	Ar	100	11	B20	Machined	Low
6	Ar	100	11	B21	As-printed	Mid
6	Ar	100	11	B22	Machined	Mid
6	Ar	100	11	B23	As-printed	High
6	Ar	100	11	B24	Machined	High
7	Ar	200	11	D7	As-printed	Low
7	Ar	200	11	D8	Machined	Low
7	Ar	200	11	D9	As-printed	Mid
7	Ar	200	11	D10	Machined	Mid
7	Ar	200	11	D11	As-printed	High
7	Ar	200	11	D12	Machined	High

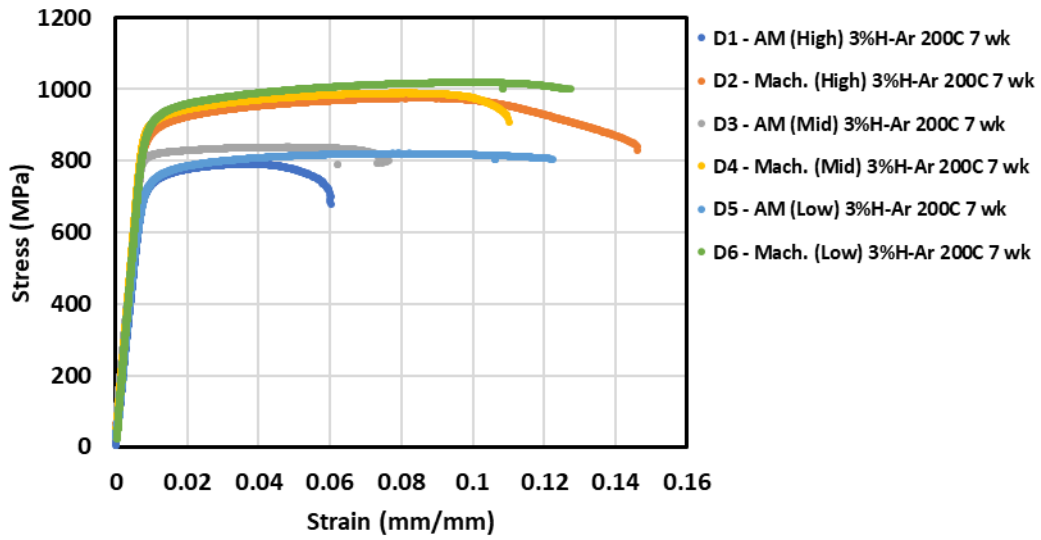


Figure 6-1 Tensile properties of vessel 1 samples, 3% hydrogen in argon, 200 °C for 7 weeks.

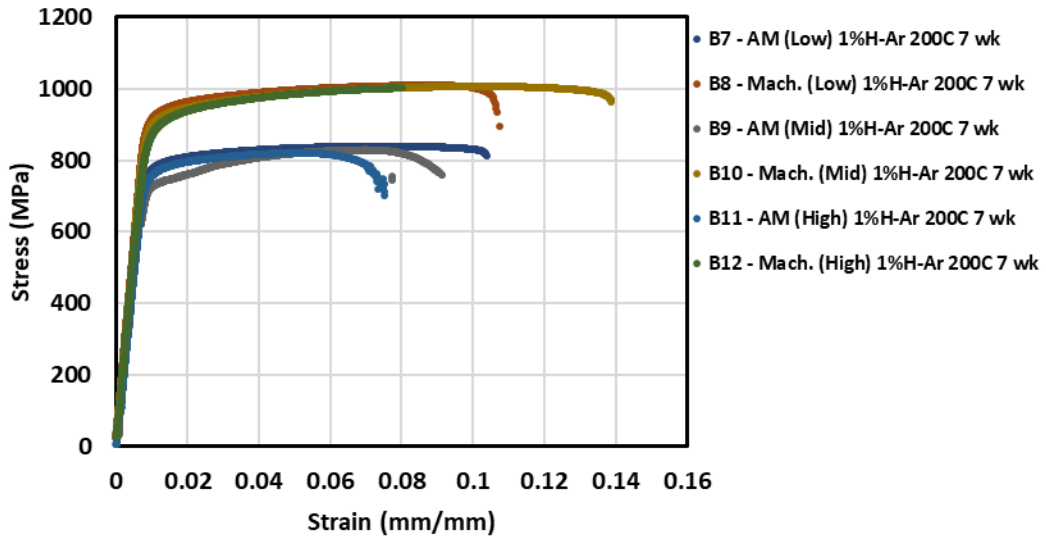


Figure 6-2 Tensile properties of vessel 2 samples, 1% hydrogen in argon, 200 °C for 7 weeks.

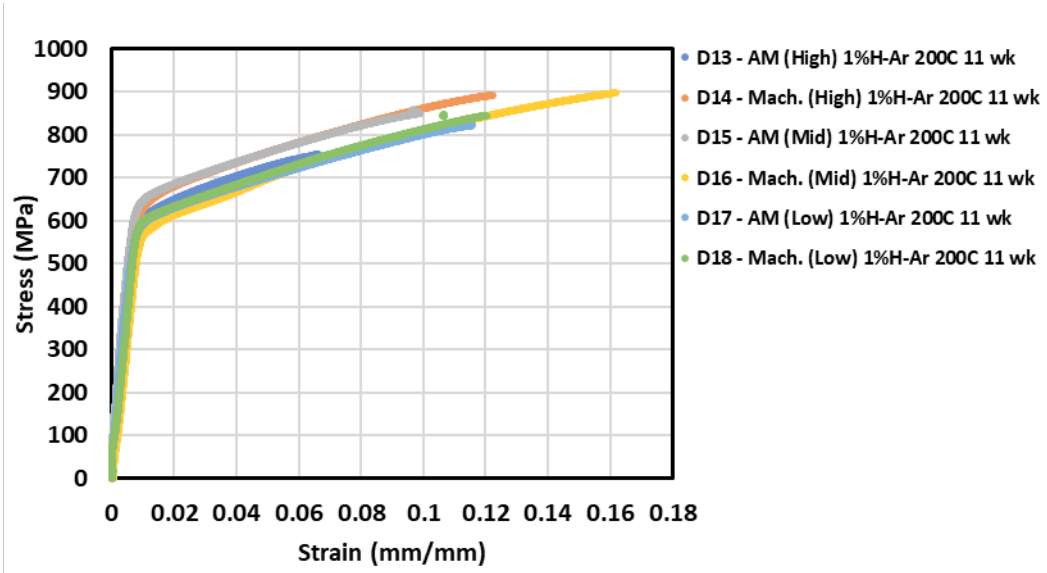


Figure 6-3 Tensile properties of vessel 3 samples, 1% hydrogen in argon, 200 °C for 11 weeks.

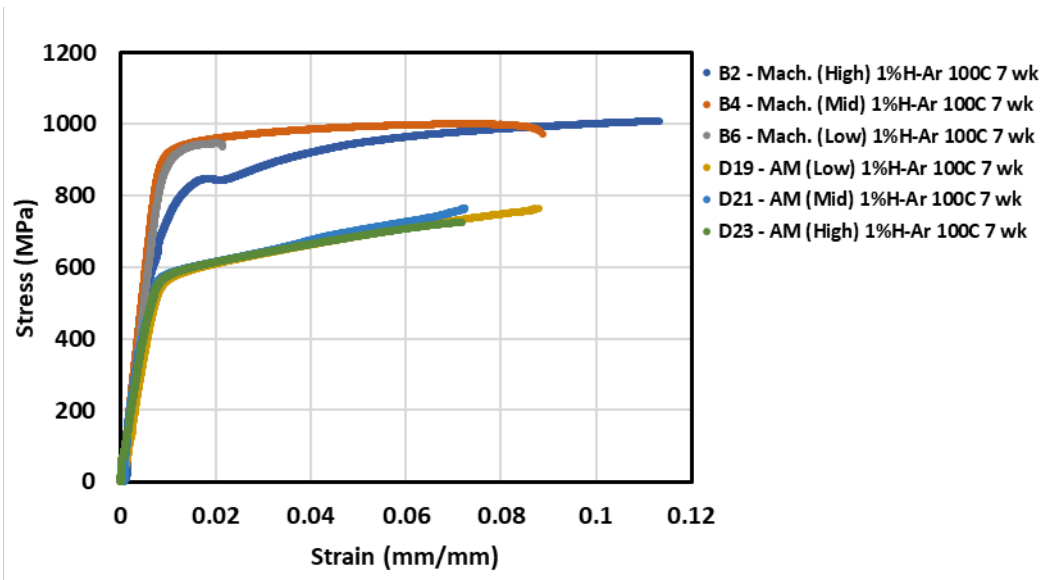


Figure 6-4 Tensile properties of vessel 4 samples, 1% hydrogen in argon, 100 °C for 7 weeks.

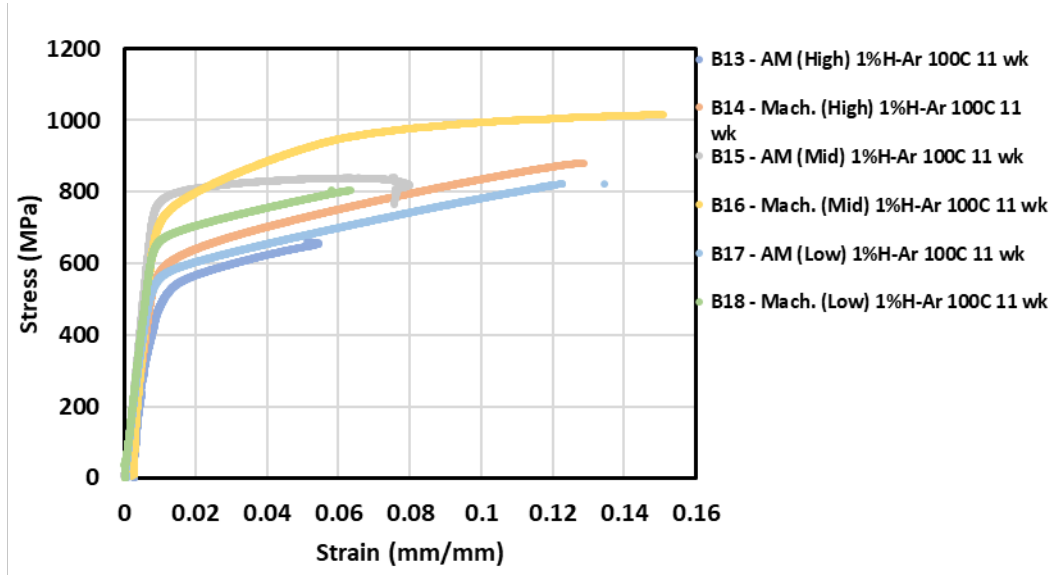


Figure 6-5 Tensile properties of vessel 5 samples, 1% hydrogen in argon, 100 °C for 11 weeks.

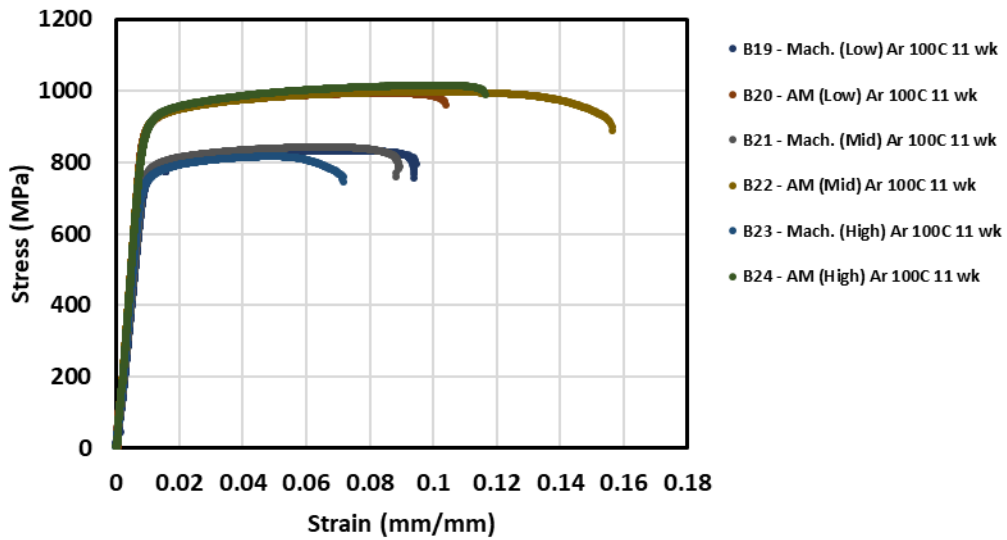


Figure 6-6 Tensile properties of vessel 6 samples, argon, 100 °C for 11 weeks.

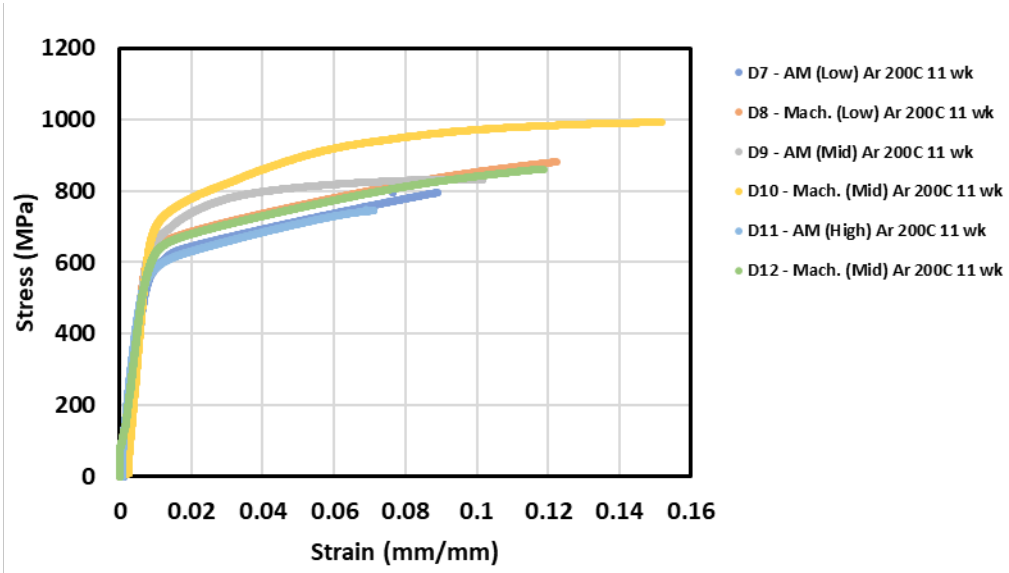


Figure 6-7. Tensile properties of vessel 7 samples, argon, 200 °C for 11weeks.

Distribution:

L. Tovo
D. Babineau
M. Rodriquiz-Martinez
P. Foster
B. Garcia-Diaz
K. Shanahan
S. Spencer
J. Bobbitt
J. McKenzie
T. Nance

